Structural and Dielectric Properties of (1-x) (Al0.2La0.8TiO3) + (x) (BiZnFeO3) (x = 0.2 - 0.8) Nanocomposites

A. Mallikarjuna
Dept. of Physics, GITAM Deemed to be University, Bangalore-562163, India
N. Suresh Kumar
Dept. of Physics, JNTUCEA, Anantapuramu, 515002, A.P, India
T. Anil Babu
Dept. of Physics, GITAM Deemed to be University, Bangalore-562163, India
S. Ramesh
Dept. of Physics, GITAM Deemed to be University, Bangalore-562163, India
Chandra Babu Naidu K (chandrababu954@gmail.com)
Dept. of Physics, GITAM Deemed to be University, Bangalore-562163, India https://orcid.org/0000-0002-0580-6383

Research Article

Keywords: Structural Transformation, Electron Microscopy, Negative Dielectric Constant, Diaelectricity, Impedance Spectroscopy

Posted Date: May 10th, 2021

DOI: https://doi.org/10.21203/rs.3.rs-493976/v1

Version of Record: A version of this preprint was published at Journal of Inorganic and Organometallic Polymers and Materials on October 11th, 2021. See the published version at https://doi.org/10.1007/s10904-021-02123-w.

Structural and dielectric properties of (1-x) ($Al_{0.2}La_{0.8}TiO_3$) + (x) ($BiZnFeO_3$) (x = 0.2 - 0.8) nanocomposites

A. Mallikarjuna[1], N. Suresh Kumar[2], T. Anil Babu[1], S. Ramesh[1]*, K. Chandra Babu Naidu[1*]
[1]Dept. of Physics, GITAM Deemed to be University, Bangalore-562163, India.
[2]Dept. of Physics, JNTUCEA, Anantapuramu, 515002, A.P, India
*Emails: sramesh664@gmail.com, chandrababu954@gmail.com

Abstract

(1-x) ($Al_{0.2}La_{0.8}TiO_3$) + (x) ($BiZnFeO_3$) (x = 0.2 - 0.8) [ALTBZFO] nanocomposites were synthesized via hydrothermal method. The X-ray diffraction patterns indicated the phase transformation from tetragonal to cubic for x = 0.2 to 0.4 - 0.8 samples, respectively. The surface morphology showed the existence of nanospheres like structures. At 1 MHz frequency also, the dielectric constant was increased from 230 to 710 for x = 0.2 – 0.6 samples, respectively. But, interestingly, x = 0.6 nanocomposite exhibited the negative dielectric behavior having the dielectric constant (ε') ~ -58.5 and dielectric loss (ε'') ~ -417 at 8 MHz. Likewise, x = 0.6 sample showed ac-electrical conductivity (σ_{ac}) -0.159 S/cm at 6 MHz. Hence, these kinds of materials can provide high charge stored capacitor, and perfect absorber applications.

Keywords: Structural Transformation; Electron Microscopy; Negative Dielectric Constant; Diaelectricity; Impedance Spectroscopy.

1. Introduction

It was a familiar fact that the perovskite nanoceramic composites performed advanced structural, and dielectric properties [1]. Even the applications of several perovskite nanocomposites were extended to biomedical, magnetic, electromagnetic, microwave, ferroelectric, charge storage etc., [1]. Few of the above merits were seen in the case of $LaTiO_3$ [2]. In the literature [1 - 4], $AlLaTiO_3$ was studied extensively by several researchers for structural, optical, morphological, electrical, and dielectric properties. The results

indicated that the huge dielectric response was obtained from the compositions of $AlLaTiO_3$. Further, the nanocomposites were synthesized including the $AlLaTiO_3$, and studied for the similar properties. These materials were of ALTBT [1], ALTBFO [5, 6], LCET [7], and AELTO [2] revealing the nanorod formation, negative dielectric behavior, and defect dipole formation, respectively. This indicated a fact that the more advanced properties were achieved on mixing the barium titanate, bismuth iron oxide, and europium oxide.

Similarly, for ALTBFO nanocomposites, the zinc element was substituted within the $BiFeO_3$ system. That is, the $BiZnFeO_3$ was mixed in the ALTBZFO nanocomposite system. In general, the ZnO is a compound having variety of applications such as wide band gap semiconductor, high conducting due to high mobility, good luminescence, etc., [8]. Due to these factors, we planned to select this compound as the substituent in the composite system thereby achieving more advanced structural, morphological, dielectric, and impedance spectroscopy properties. In addition, $BiFeO_3$ showed the biosensor [9], magnetoelectric [10], optical [11], magnetic [12], multiferroic [13], enhanced electrical properties [13], and high dielectric constant [14]. Further, it was also noticed in the literature that the $BiZnFeO_3$ provided photovoltaic [15] and progressed magnetic properties [16]. In case of Zn-doped $BiFeO_3$, the leakage, and high polarization behavior was observed predominantly [17]. Similarly, there was a significant influence on optical, electrical, and magnetic properties upon doping the zinc in the bismuth iron oxide perovskite system [18 - 20]. Uniyal et al. [21], reported the multiferroic nature of $ZnFe_2O_4$–$BiFeO_3$ nanocomposites. Hence, the ALTBZFO nanocomposites were prepared using hydrothermal method owing to the benefits such as low operating temperature, less time & power consuming, well crystallinity, low particle size, etc., [1].

2. Materials and Methods

For the synthesis of (1-x) ($Al_{0.2}La_{0.8}TiO_3$) + (x) ($BiZnFeO_3$) (x = 0.2 - 0.8) [ALTBZFO] nanocomposites, the hydrothermal method was preferred. As a part of this, the raw materials were considered to be $Al(NO_3)_3$.$9H_2O$ (99.8 % purity, Sigma-Aldrich), $La(NO_3)_3.6H_2O$ (99.8 % purity, Sigma-Aldrich), $Bi(NO_3)_3{\cdot}5H_2O$ (99.8 % purity, Sigma-Aldrich), $Fe(NO_3)_3{\cdot}9H_2O$ (99.9 % purity, Sigma-Aldrich), $Zn(NO_3)_2$. $6H_2O$ (99.9 % purity, Sigma-Aldrich), and TiO_2 (99.9 % purity, Sigma-Aldrich). These precursors were taken in a stoichiometric ratio and kept in a cleaned glass beaker. Further, the mixture was dissolved in distilled water, and stirred for half an hour at room temperature by maintaining stirring rate of 450 rpm. As a result of this, a delicious solution was formed, and it was kept in well cleaned Teflon bowl of 300 ml capacity. This bowl was again placed in a stainless-steel autoclave. Then, the autoclave was kept in a hot air oven, and further the reaction was taken place at 150^{o}C/6 hr. After completion of reaction, the autoclave was quenched to room temperature. Then, the Teflon bowl was removed from the autoclave to extract the nanocomposite solution. This solution was washed for 10 times, and further dried for 2 hr., at 60^{o}C. Thus, the final nanocomposite product was obtained for x = 0.2 – 0.8 samples (Fig.1). In the next step, the nanocomposites were subjected to various analysis works like X-ray diffractometer (XRD, Bruker, $Cu_{K\alpha}$, λ = 0.15406 nm), transmission electron microscope (TEM: Model Tecnai G20, FEI, USA), field-emission scanning electron microscope (FE-SEM, Ultra 55, Carl Zeiss), and LCR controller (HIOKI 3532-50, 42 Hz–8 MHz) to study the structural, morphological, and dielectric properties, respectively.

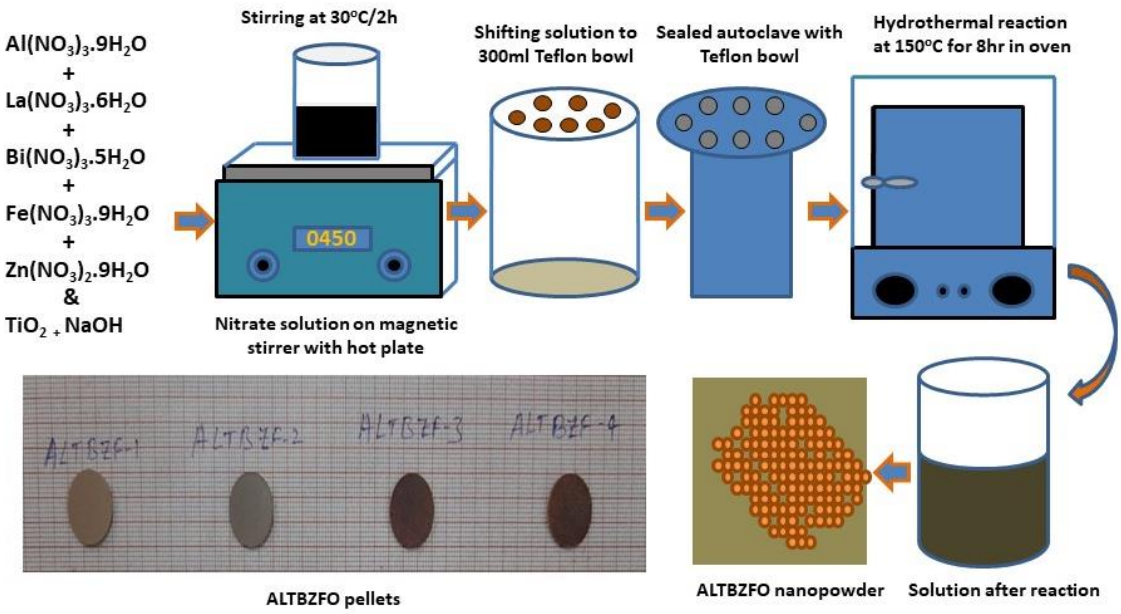

Fig.1. Schematic representation of hydrothermal synthesis and sample preparation

3. Results and discussion

The X-ray diffraction patterns of ALTBZF [(1-x) ($Al_{0.2}La_{0.8}TiO_3$) + (x) ($BiZnFeO_3$) (x = 0.2 - 0.8)] nanocomposites were recorded by considering the two-theta angle on X-axis and the corresponding intensity all reflection planes on Y-axis. From Fig.2, it was observed that all the nanocomposites showed well crystalline nature. It was also seen that the maximum intensity of x = 0.2 sample showed at 2θ = 25.463°, while the x = 0.4 - 0.8 samples revealed the maximum intensity at 2θ = 31.421°. This established a fact that there was a phase transition from x = 0.2 to 0.4 - 0.8. All the diffraction positions of x = 0.2 – 0.8 composites were compared with standard JCPDS. Then it was observed that the x = 0.2 sample showed the reflection planes comparable to the JCPDS: 21 – 1272, while x = 0.4 – 0.8 nanocomposites contain the reflections comparable to the JCPDS: 86 – 0368. This comparison confirmed a fact that the x = 0.2 sample achieved the tetragonal structure, whereas the x = 0.4 – 0.8 samples showed the cubic phases. In addition, the secondary phases related to the $BiFeO_3$ (indicated by *) and La_2TiO_5 (indicated by +) were noticed. Usually, this kind of secondary phase formation was attributed to the vast difference of ionic radii of cations present in the composite system. That is, La^{+3}: 0.136 nm, Bi^{+3}: 0.096 nm, Al^{+3}: 0.039

nm, Ti^{+4}: 0.068 nm, Fe^{+3}: 0.0645 nm, and Zn^{+2}: 0.060 nm [22]. Herein, the bismuth, and lanthanum cations have larger ionic radii as compared with the rest of the cations. Therefore, bismuth, and lanthanum cations can form their associated compounds ($BiFeO_3$ and La_2TiO_5). The high crystallinity was also identified for all diffraction planes. Further, the average crystallite diameter was calculated using the Scherrer relation [23]: D_a: $0.9\lambda/\beta Cos\theta$, where λ indicates the wavelength of X-rays used (0.15418 nm), β is full width half maxima (FWHM) and θ is the angle of diffraction. The results indicated that the D_a was found to be increasing from 75.3 to 160.3 nm for x = 0.2 – 0.6, respectively, while for x = 0.8, it was noticed to be 107.4 nm (decreased). This kind of manner was attributed to the decrease of FWHM (from 0.443 – 0.104 radian) for x = 0.2 – 0.6 samples, and further it was increasing to 0.109 radian. This revealed a fact that there exists an inversely proportional relationship with between FWHM and D_a. Afterwards, the lattice parameters (a, b & c) were determined using the relations [5, 24, 25]: $1/d^2 = (h^2+k^2)/a^2 + l^2/c^2$ (for tetragonal) and $1/d^2 = (h^2+k^2+ l^2)/a^2$ (for cubic). The obtained results indicated that for x = 0.2 sample, a = b = 3.774 Å & c = 9.395 Å (Table. 1). On the other hand, for x = 0.4 – 0.8 samples expressed the decreasing trend from 12.761 to 12.714 Å, respectively. These results clearly indicated that the structural transformation was occurred from tetragonal to cubic for x = 0.2 to 0.4/0.6/0.8 samples. Similarly, the unit cell volume (V) was found to be 133.81 $Å^3$ for x = 0.2 while the same parameter was decreased from 2078.1 to 2055.2 $Å^3$, for x = 0.4 – 0.8, respectively. Furthermore, the X-ray density values were calculated using a formula: ρ_x (g/c.c.) = Z*C.M.W./(N*V) (for tetragonal Z = 4 & for cubic Z = 1), where Z = effective number of atoms per unit cell, C.M.W is the composite's molecular weight, N is the Avogadro's number ($6.023x10^{23}$), and V is the unit cell volume [5]. The ρ_x of x = 0.2 was about 12.187 g/c.c., while the similar parameter was increased from 0.223 to 0.279 g/c.c., for x = 0.4 – 0.8 samples, respectively. This kind of behavior was attributed to the increasing trend of

composite molecular weight (C.M.W.) from 245.55 to 345.04 g/mole. Moreover, the specific surface area (S) was noted to be very low for x = 0.2, whereas for x = 0.4 – 0.8 samples, it was found to be changing from 149.7 to 248.3 m^2/g. The high 'S' values usually indicate the advanced electrical properties.

Table.1 XRD parameters of ALTBZF nanocomposites.

x	0.2	0.4	0.6	0.8
D_a (nm)	75.3	108.5	160.3	107.4
FWHM (radian)	0.443	0.111	0.104	0.109
a = b (Å)	3.774	12.761	12.747	12.714
c (Å)	9.395	12.761	12.747	12.714
V $(Å)^3$	133.81	2078.1	2071.2	2055.2
C.M.W (g/mole)	245.55	278.71	311.88	345.04
ρ_x (g/c.c.)	12.187	0.223	0.250	0.279
S (m^2/g)	6.538	248.3	149.7	200.4

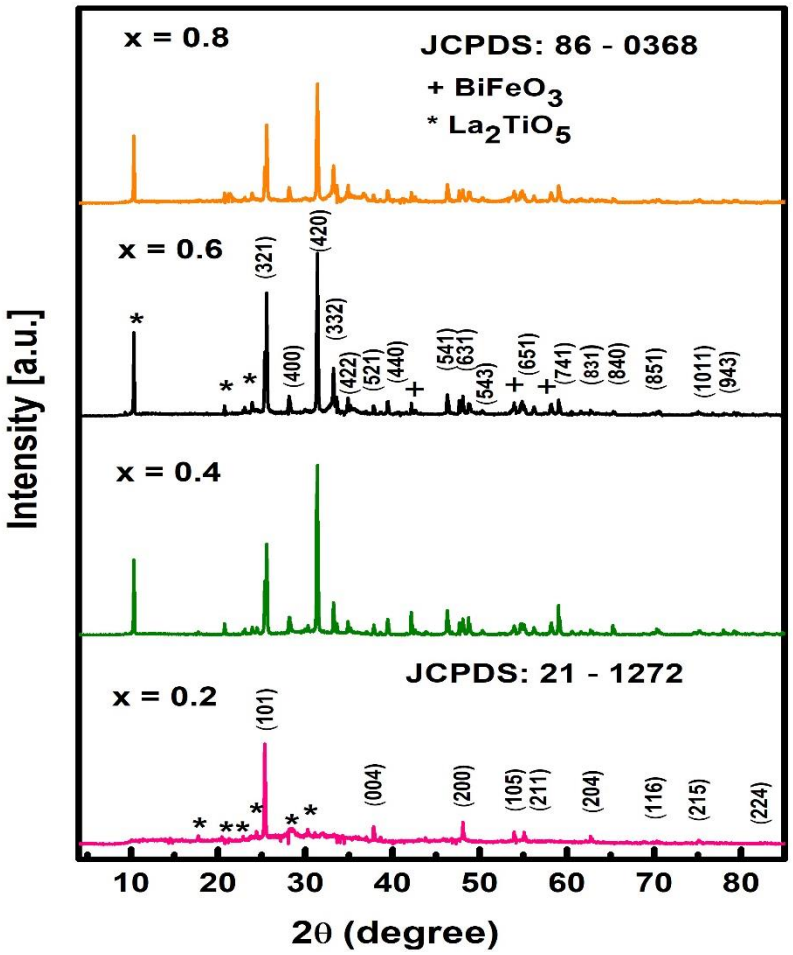

Fig.2 XRD patterns of ALTBZF nanocomposites

The surface morphology of ALTBZF nanocomposites was analyzed using the field emission scanning electron microscopy (FESEM), and transmission electron microscopy (TEM) pictures. The FESEM pictures were shown in Fig.3 at 100 nm scale. In Fig.3, it was observed that the larger numbers of cotton spheres like grains were formed for x = 0.2. Moreover, few nanofibers like grains were also deposited in the microstructure. It was also noticed that the distribution of cotton spheres was almost homogeneous. For x = 0.4 samples, the bigger sized and well-defined cotton spheres were seen. But for x = 0.6 sample exhibited the clustered like grains possessing the asymmetrical cotton spheres. On the other hand, the x = 0.8 sample revealed the existence of cotton spheres in limited number covered by smaller nanofibers. It was understood that with an increase of $BiZnFeO_3$ in the composite system, the morphology was changed from larger numbers of cotton spheres to smaller nanofibers including limited numbers of cotton spheres. In the same way, the TEM pictures were recorded as provided in Fig.4. From TEM pictures, we noticed that x = 0.2 – 0.6 samples exhibited the formation of symmetrical nanospheres including small nanofibers. On the other hand, x = 0.8 sample showed the presence of nanospheres including larger nanofibers as compared with x = 0.2 – 0.6 samples. The similar kind of morphology was observed in the FESEM pictures also. Further, the average particle size was measured and found to be altering from 115 to 166 nm for all the nanocomposites. Even the selected area electron diffraction patterns (SAED) (Fig.5) were recorded and showed the presence of concentric circular rings with good intensity. These diffraction rings agreed with X-ray diffraction patterns.

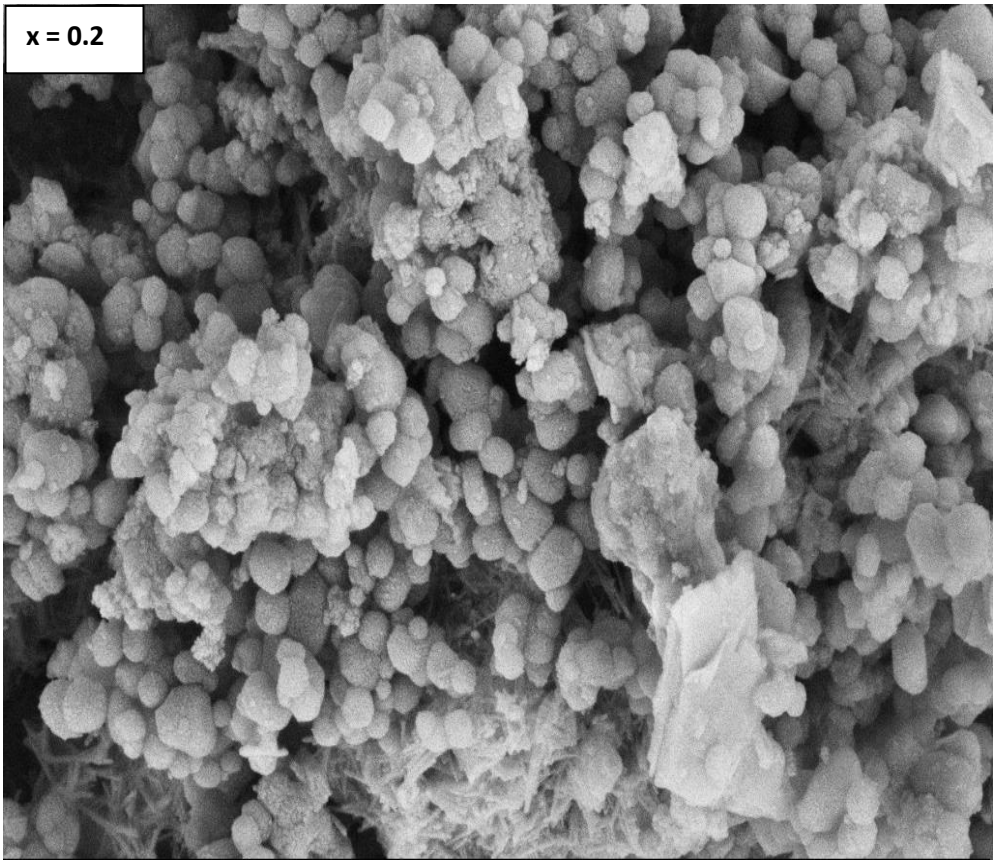
x = 0.2

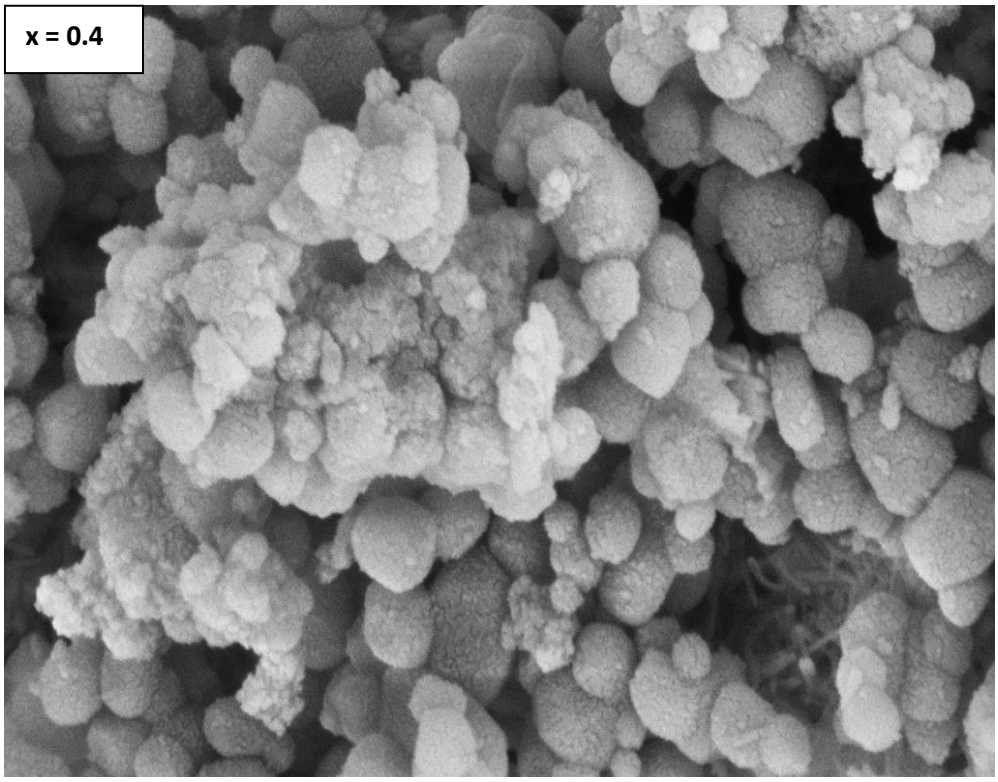
x = 0.4

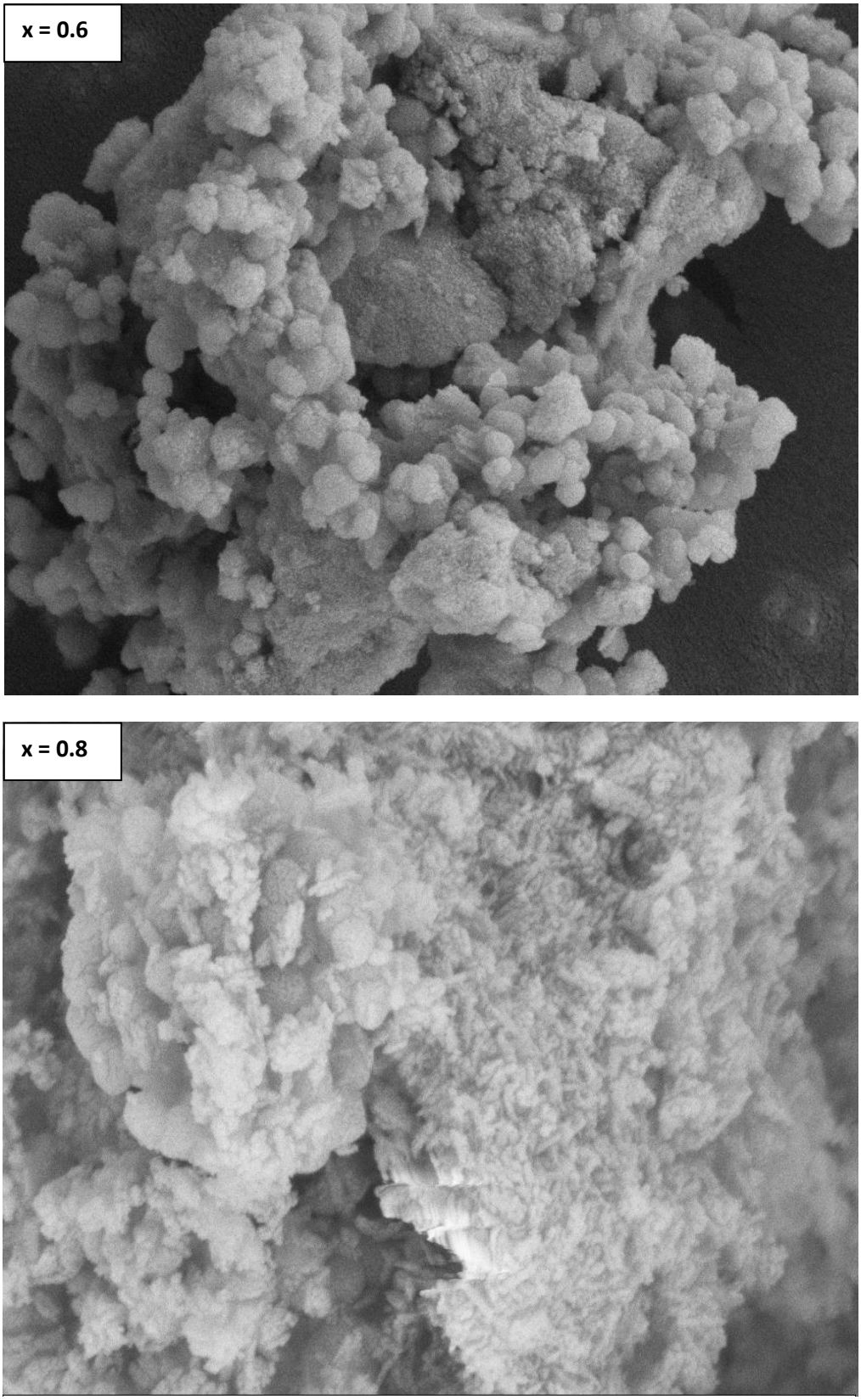

Fig.3 FESEM pictures of ALTBZF nanocomposites

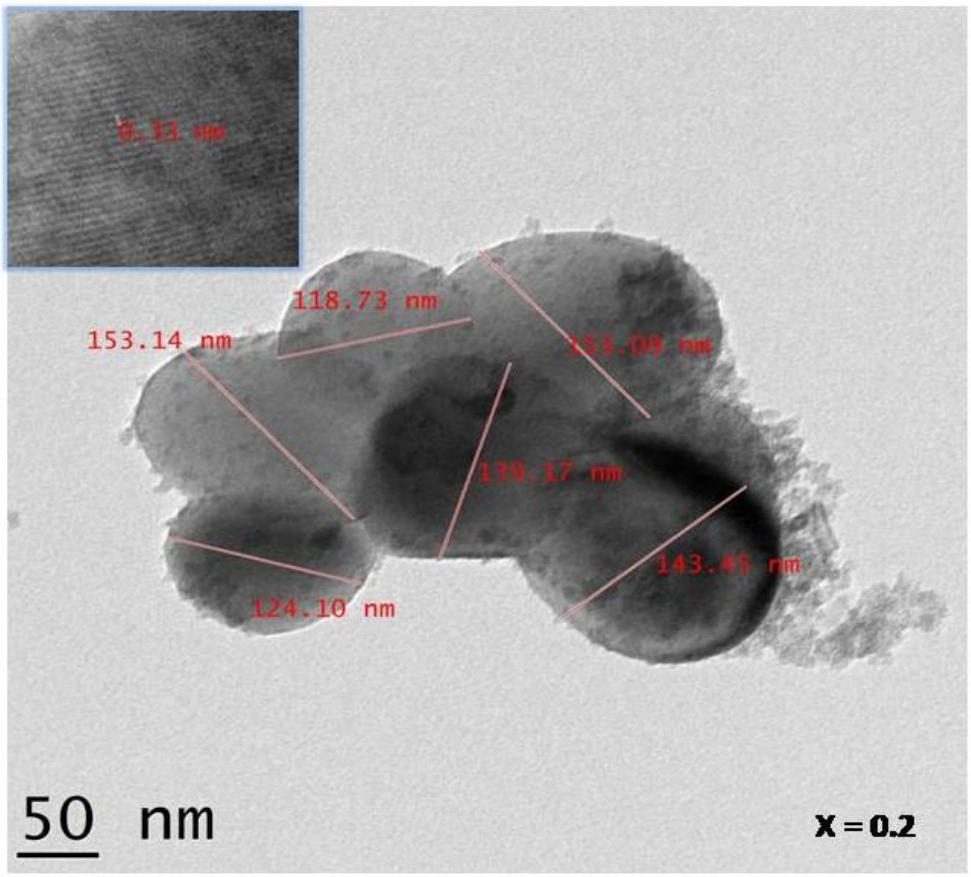
0.33 nm
118.73 nm
153.14 nm
153.09 nm
139.17 nm
143.45 nm
124.10 nm
50 nm
X = 0.2

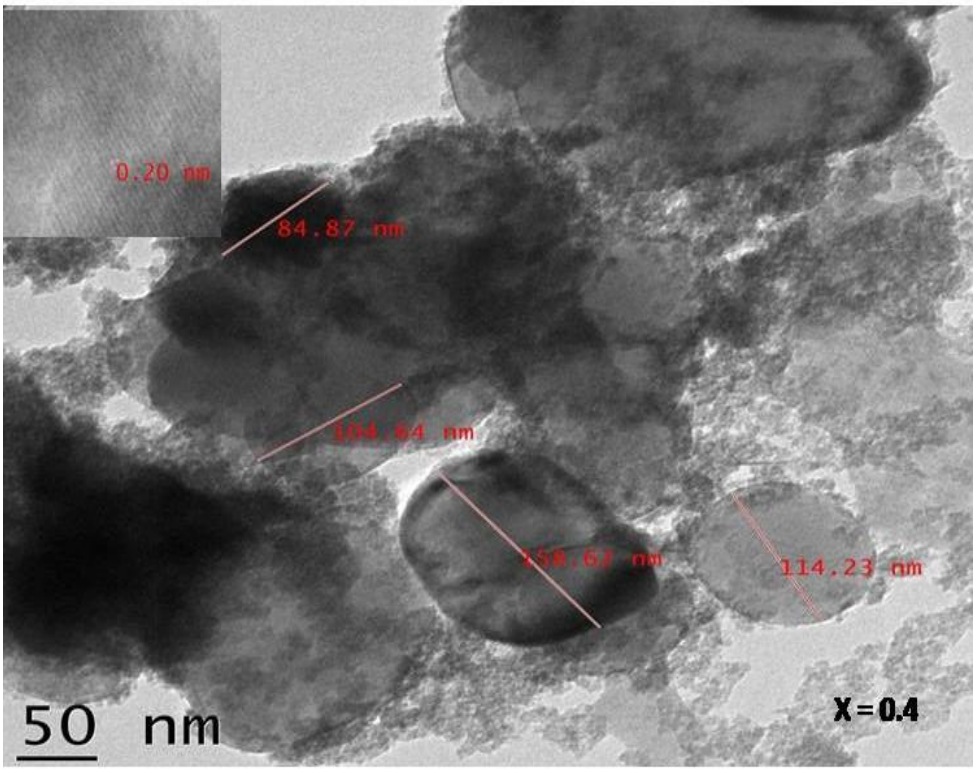
0.20 nm
84.87 nm
104.64 nm
150.67 nm
114.23 nm
50 nm
X = 0.4

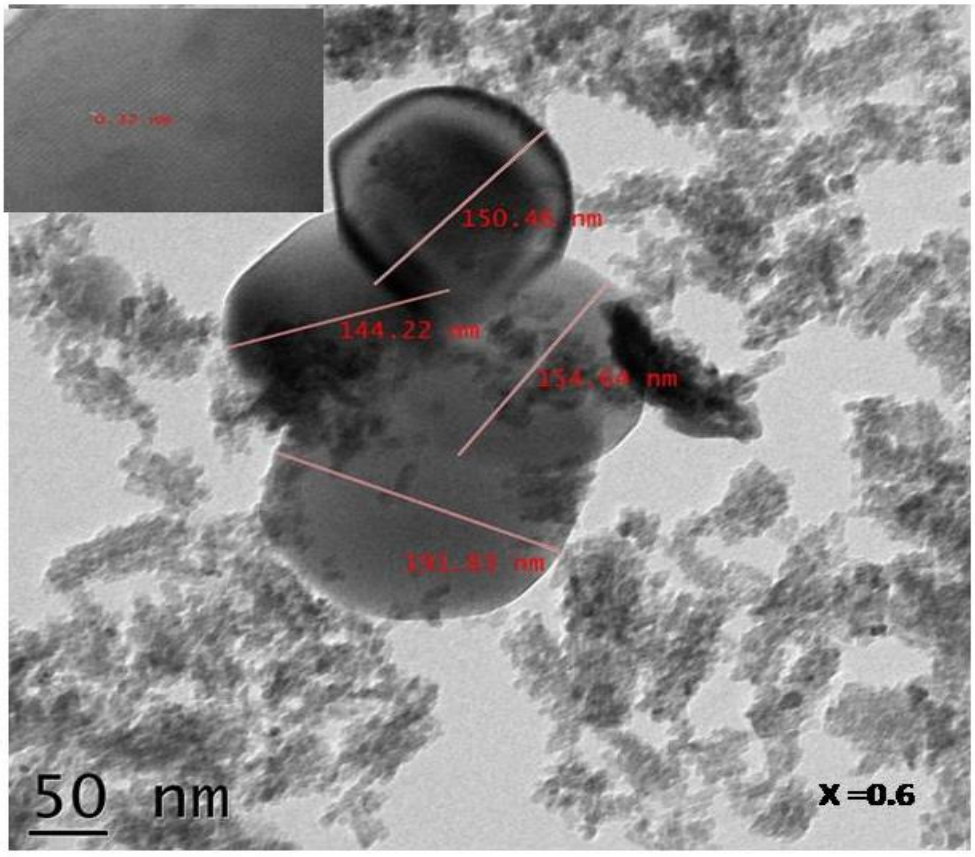

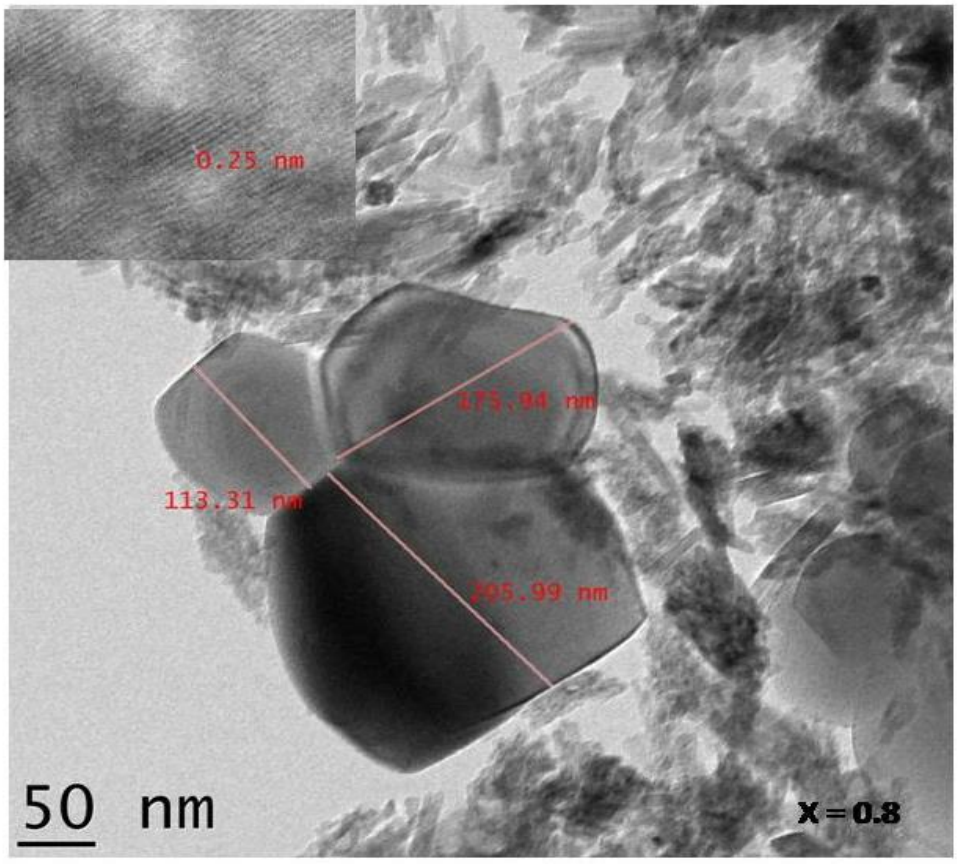

Fig.4 TEM pictures of ALTBZF nanocomposites

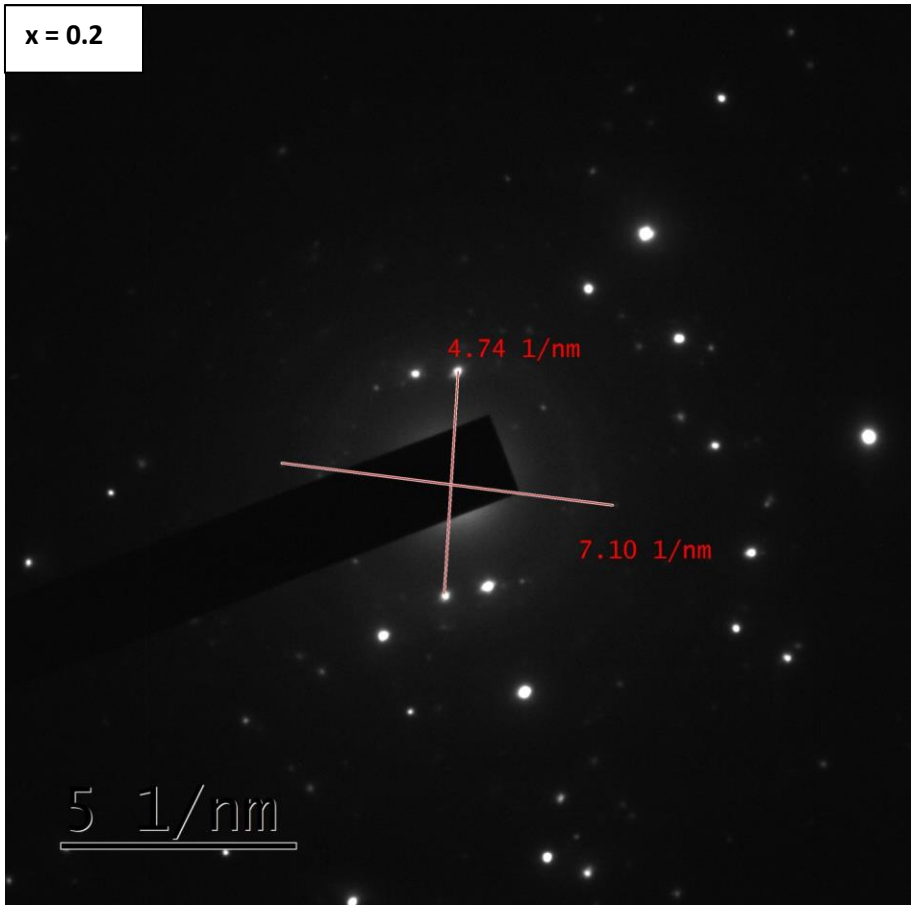
x = 0.2
4.74 1/nm
7.10 1/nm
5 1/nm

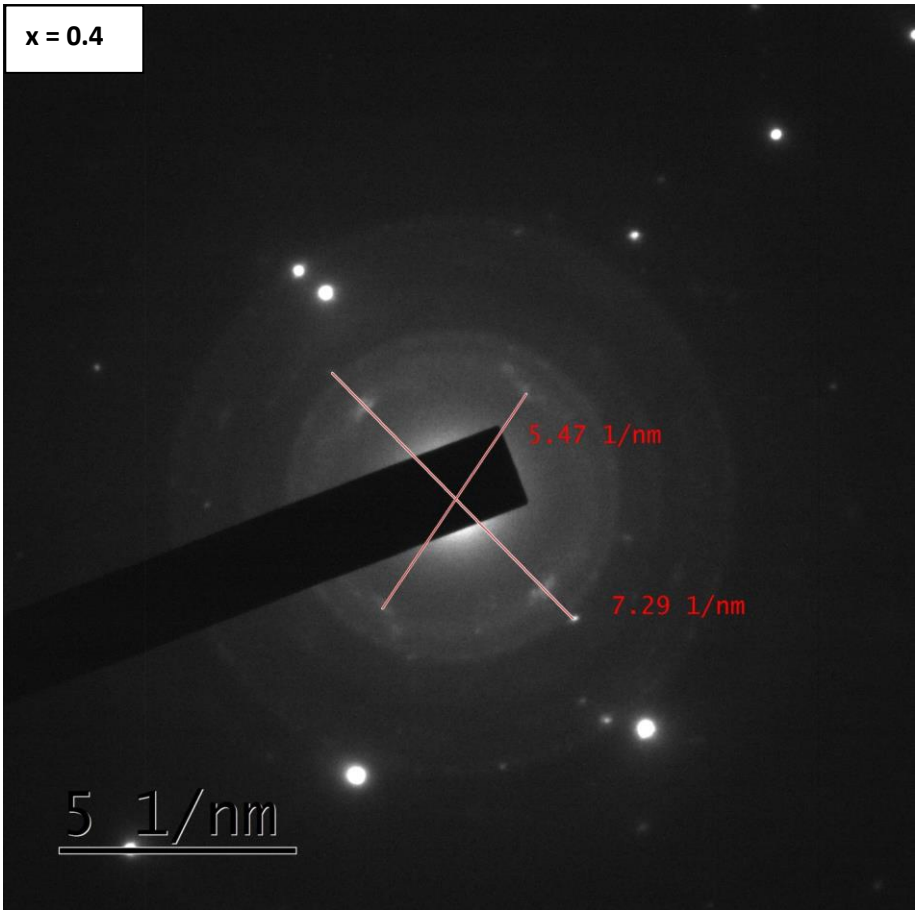
x = 0.4
5.47 1/nm
7.29 1/nm
5 1/nm

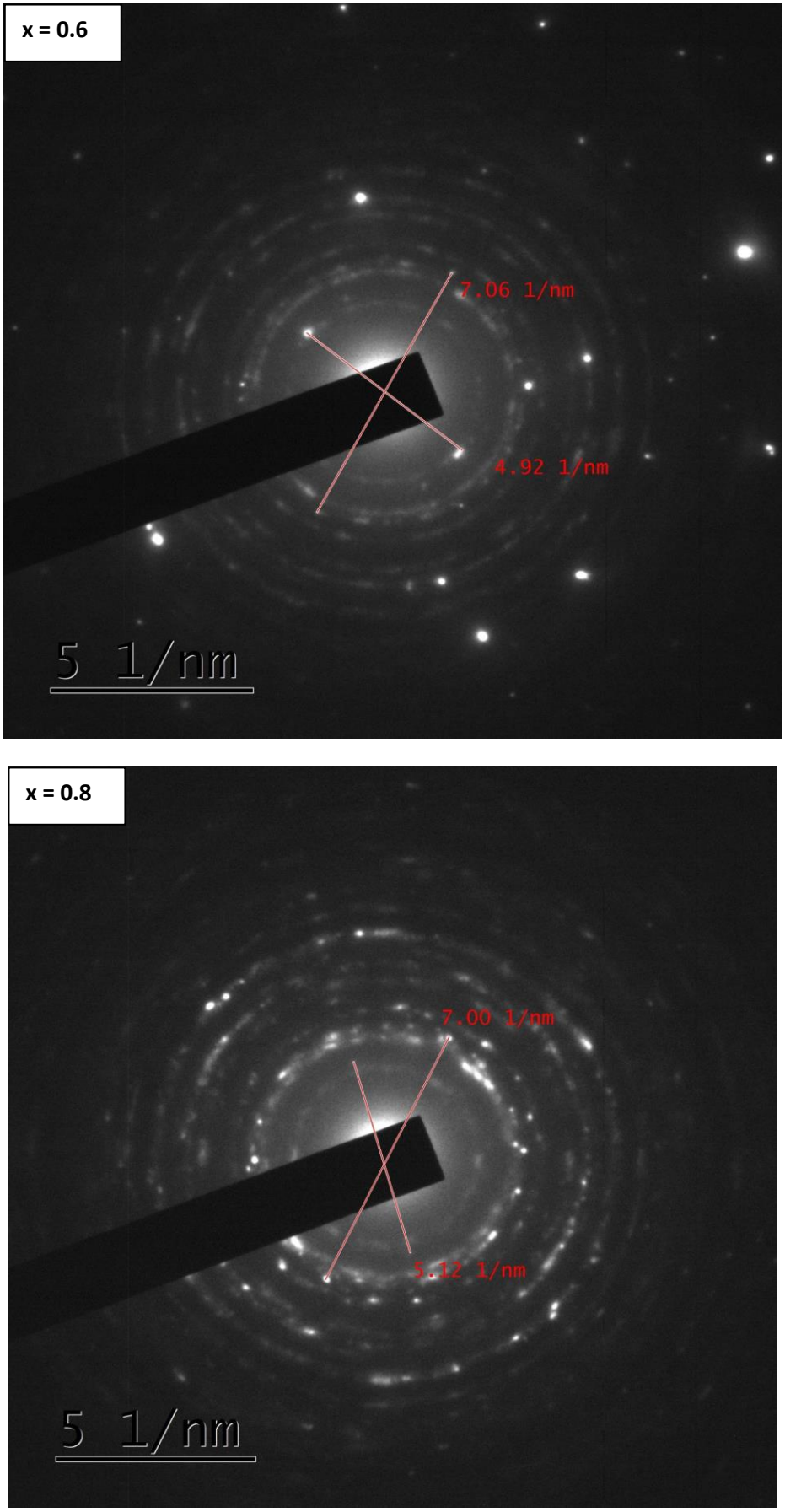

Fig.5 SAED patterns of ALTBZF nanocomposites

The dielectric behavior of ALTBZFO nanocomposites was explained using the dielectric constant (ε'), and dielectric loss (ε") versus frequency (log ω) plots. In Fig.6 (ε' - log ω), it was seen that the ε' was very high for x = 0.2 – 0.8 samples. Usually, this kind of behavior can be attributed to the space charge species. That is, the charges will be piled up at the grain boundary interface at low log ω. Thus, the polarization can be developed progressively, and it can be treated as Maxwell-Wagner's polarization [26]. It leads achieving the high dielectric constant. It was seen from the ε' - log ω plots that the ε' was found to be increasing from 3727 to 14166 for x = 0.2 – 0.6 samples (Table.2), respectively at 1 kHz. But for x = 0.8 sample, it was decreased to 5081. Similarly, the ε" (in Fig.6 (ε" - log ω)) also showed the increasing trend from 566 to 15340 for x = 0.2 – 0.6 samples, respectively. But for y = 0.8, it was reduced to 1509. At 1 MHz frequency also, the similar increasing trend was occurred from 230 to 710 for x = 0.2 – 0.6 samples, respectively. For x = 0.8, it was decreased to 252. From 6 to 8 MHz also, the similar behavior was observed for all nanocomposites except for x = 0.6. For all the samples, the dielectric relaxations were noticed in the dielectric loss versus frequency plots at log ω = 5 to 6.35. These relaxations were formed normally, due to the accumulation of charges at the interface of sample. Moreover, interestingly, x = 0.6 sample showed negative dielectric behavior having the ε' ~ -58.5 ε" ~ -417 (Table.2). This indicated a fact that for x = 0.6 sample, the transition was happened from positive to negative dielectric behavior at 6 MHz frequency. In general, it was known that the positive dielectric behavior is a usual property while the negative dielectric behavior is an unusual property. This kind of property was earlier observed in the case of perovskite materials [27, 28] as well as the metamaterials [2, 7, 29 - 33]. However, the present nanocomposites are not the metamaterials. But nevertheless, the negative dielectric behavior can be obtained due to the geometrical effect thereby providing the negative polarization. That is, for the provided electric field frequency, the charge carriers will be aligned in the

opposite direction of the applied electric field. Therefore, the polarization will be developed having negative sign. This can lead to the formation of negative polarization. Consequently, the negative dielectric constant, and dielectric loss will be achieved. This behavior can be considered as diaelectricity nature which is like the diamagnetism [2]. That means, in case of diamagnetic nature of a magnetic specimen, the magnetization will be developed opposite to the direction of applied magnetic field. Likewise, the in case of diaelectricity, the polarization will be developed opposite to the direction of applied electric field frequency. The similar observations were evidenced in the case of x = 0.6 nanocomposite during 6 – 8 MHz frequency. From these results, it was understood that the nanocomposites (x = 0.2, 0.4, and 0.8) exhibiting the high dielectric constant can be suited for high charge storage capacitor applications [2]. Likewise, the x = 0.6 sample offering negative dielectric behavior can provide applications in waveguides, filters, antenna, electromagnetic cloaking devices, and perfect microwave absorbers [2]. Further, the ac-electrical conductivity was calculated using a relation σ_{ac}: $\varepsilon_o\varepsilon"\omega$, where ε_o is the permittivity of free space, and the other symbols have their usual meaning [34]. To explain the electrical conductivity as a function of composite and frequency, the log σ_{ac} versus log ω plots (Fig.7) were drawn. It was clear that at low log ω value, the σ_{ac} was very small while going to the high log ω values, the conductivity was increased progressively. This was happened for y = 0.2, 0.4, and 0.8 samples. But for x = 0.6 sample, the ac-electrical conductivity was noticed to be negative from 6 to 8 MHz frequency. At 1 MHz, the σ_{ac} was found to be varying from 0.0142 to 0.0976 S/cm for all nanocomposites. This indicated that the high conductivity was noticed for all the samples at room temperature (at 1 MHz). For x = 0.6 sample, the σ_{ac} showed -0.159 S/cm at 6 MHz (Table. 3). This manner was inferred due to the negative dielectric loss of the same sample.

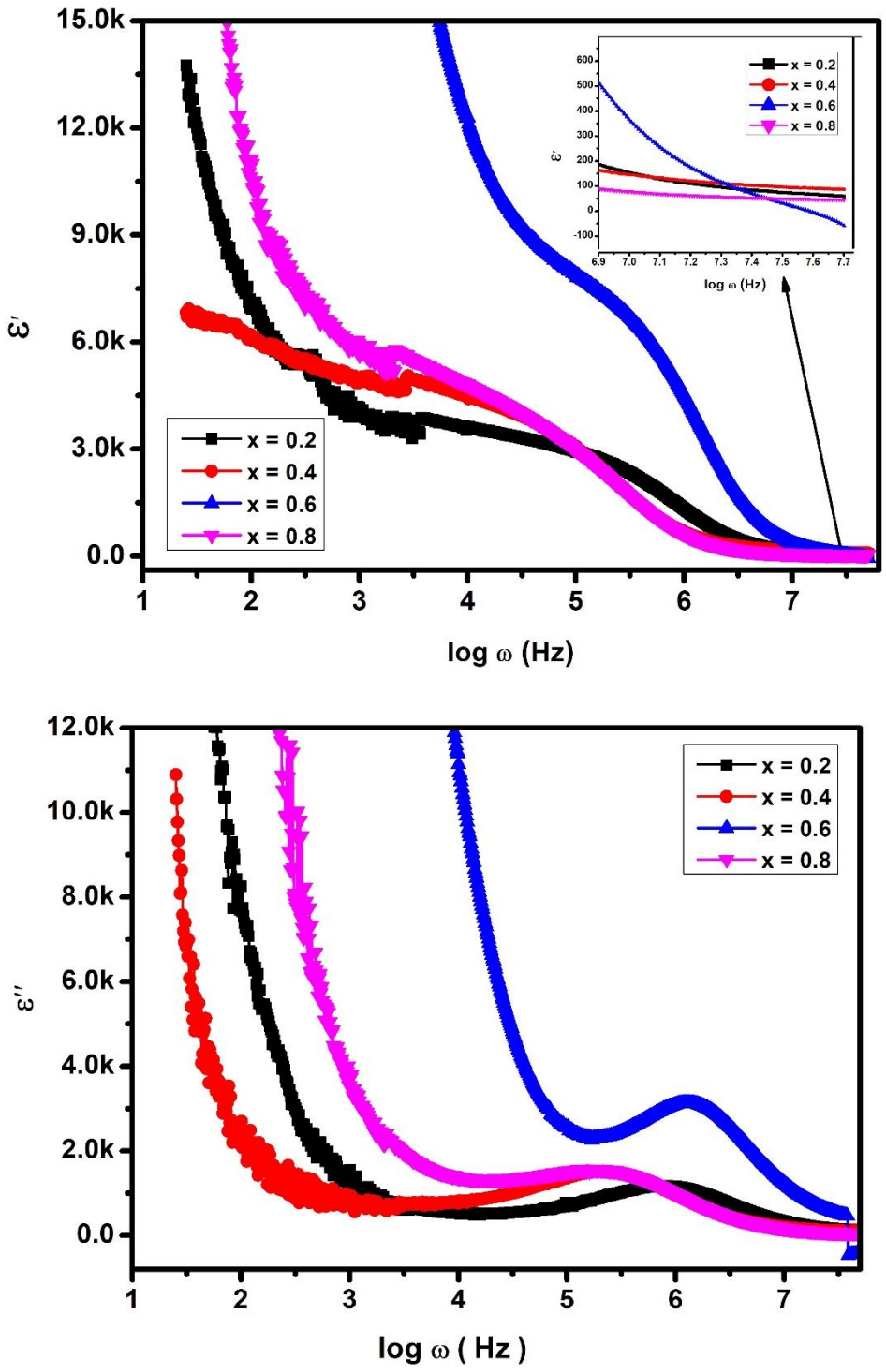

Fig.6 Frequency dependence of dielectric properties of ALTBZF nanocomposites

Table.2. Dielectric parameters of ALTBZF nanostructures at different frequencies

x	0.2		0.4		0.6		0.8	
frequency	ε'	ε"	ε'	ε"	ε'	ε"	ε'	ε"
1 kHz	3727	566	4700	755	14166	15340	5081	1509
10 kHz	3123	646	3457	1226	8292	3715	3424	1415

100 kHz	1771	1154	1013	1198	5565	2864	975	1237
1 MHz	230	470	183	271	710	1729	103	252
2 MHz	127	280	132	172	254	1029	69	143
3 MHz	98	209	112	135	128	751	58	105
4 MHz	82	174	102	119	69	603	53	86
5 MHz	74	152	95	110	31	513	49	75
6 MHz	68	142	92	107	**-2.4**	**-457**	48	70
7 MHz	64	139	89	108	**-26.1**	**-432**	46	67
8 MHz	58	142	87	114	**-58.5**	**-417**	45	68

Table.3. AC-electrical conductivity of ALTBZF nanostructures at different frequencies

x	0.2	0.4	0.6	0.8
frequency	σ_{ac} (S/cm)			
1 MHz	0.0265	0.0153	0.0976	0.0142
6MHz	-	-	**-0.159**	-
7MHz	-	-	**-0.1703**	-
8MHz	-	-	**-0.187**	-

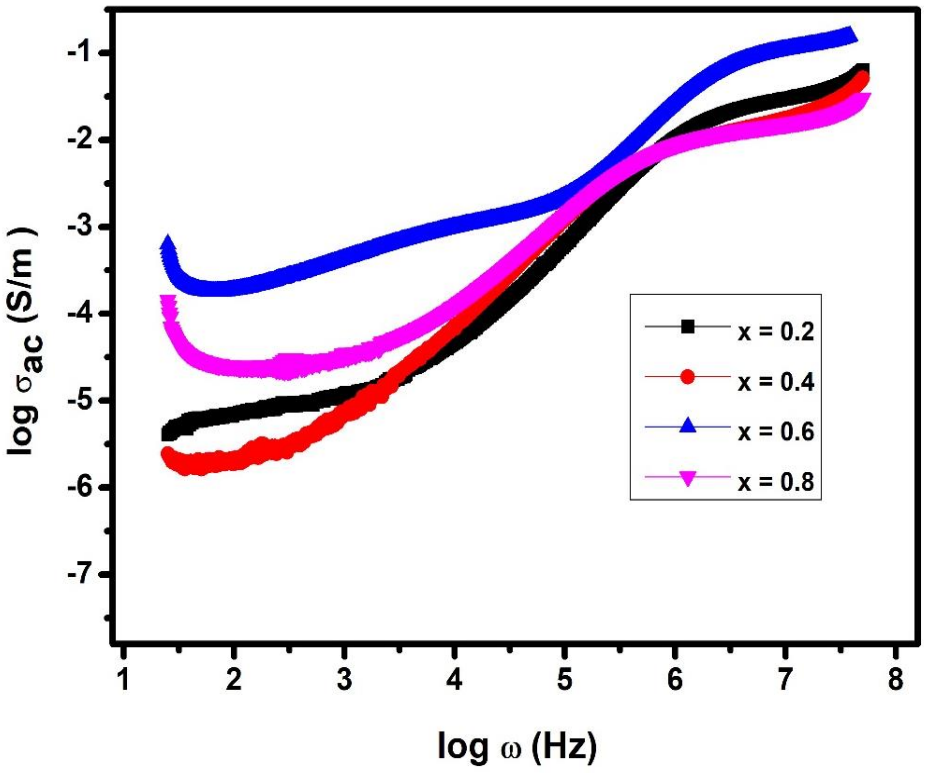

Fig.7 AC- electrical conductivity versus log ω plots of ALTBZF nanocomposites

To analyze the microstructure, electrical conduction, and polarization mechanisms, the impedance analysis was carried out. For this, the complex impedance (Z* = Z'-jZ"), wherein the Z' is the real, and Z" is the imaginary part. In Fig.8, the variation of Z', and Z"

was provided as a function of log ω. The Z', and Z" values are very high at low log ω values. This behavior was obtained owing to the space charge effect. That is, the charge carriers will be accumulated at the interface, and therefore, this trend can lead to the high magnitude of Z', and Z" values. Moreover, at high log ω values, the Z', and Z" parameters were decreased to small values. This can indicate a fact that the effect of charge species was decreased at high frequencies. The Cole-Cole plots (Z' versus Z") were shown in Fig.9. For all the samples, the Cole-Cole plots showed the formation of single, and partial semicircular arcs. In general, the partial arcs will be formed due to the long-range motion of the charge carriers [34]. But for x = 0.6, the reverse nature of arc was observed at high frequencies. This manner was occurred due to the diaelectricity behavior at frequencies. The dielectric modulus spectrum was analyzed using M' – log ω, M" – log ω, and M' versus M". In the M' – log ω, and M" – log ω plots (Fig.10) [$M' = \varepsilon'/(\varepsilon'^2+\varepsilon''^2)$ (real part), and $M'' = \varepsilon''/(\varepsilon'^2+\varepsilon''^2)$ (imaginary part)], it was found that the M', and M" values showed almost zero value at low log ω. This behavior was attributed to the lack of control of mobility of charges and not having the restoring force to the charges to attain their original position [2]. For further increase of frequency, M', and M" values were increased sharply. This was attributed to the mobility of charges for short distances [2]. There were no considerable relaxations in the M' – log ω, M" – log ω plots. The M' versus M" plots (Fig.11) ensured that the single, and partial semicircular arcs were seen for x = 0.2 – 0.8 nanocomposites. At high frequencies, the x = 0.6 sample showed the complete reverse nature of arc indicating the diaelectricity behavior. The similar observations were noticed in the literature [2, 7, 27, 28]. The partial arcs were formed due to the partial relaxation strength.

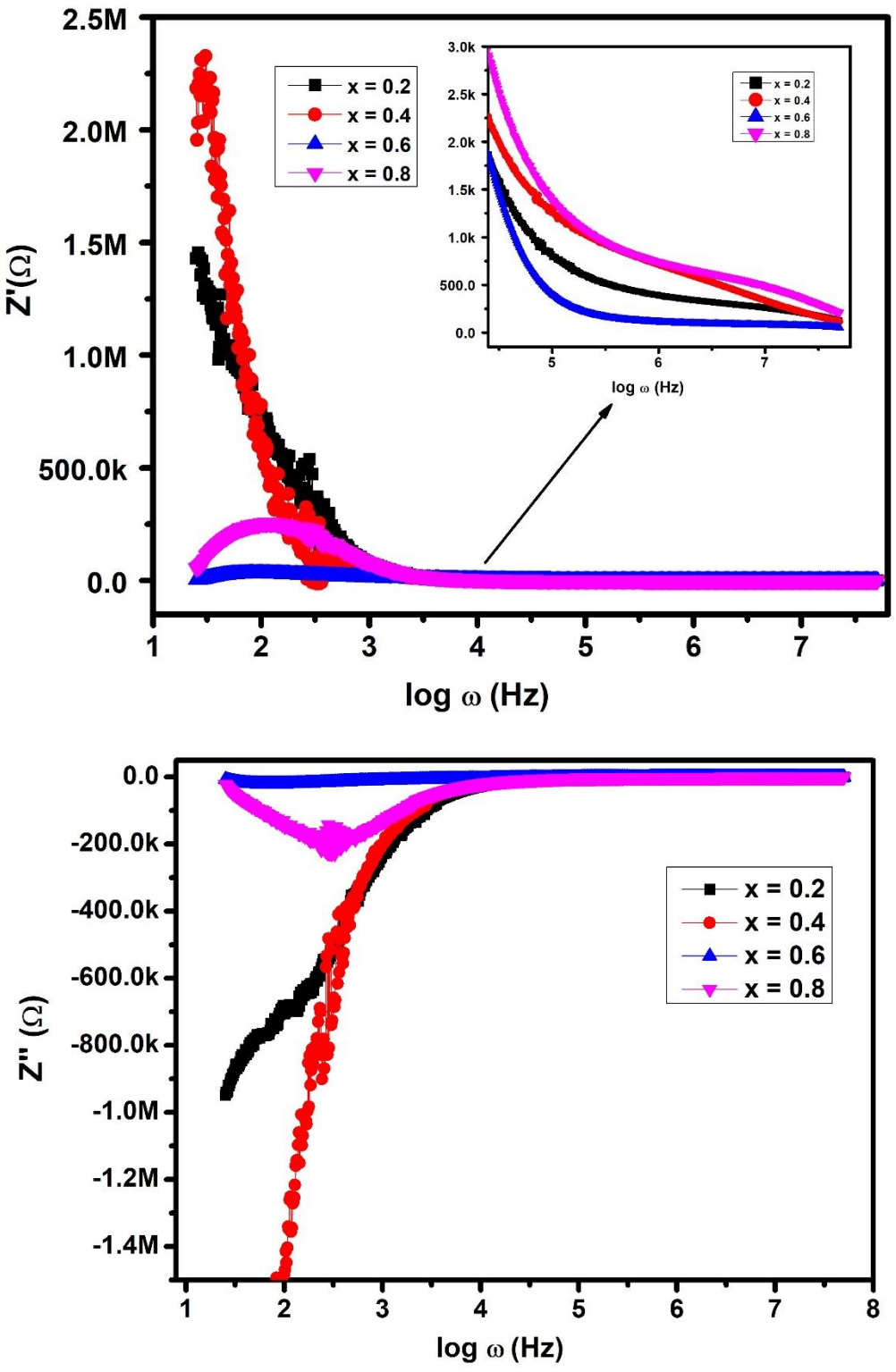

Fig.8 Z'- log ω and Z''- log ω plots of ALTBZF nanocomposites

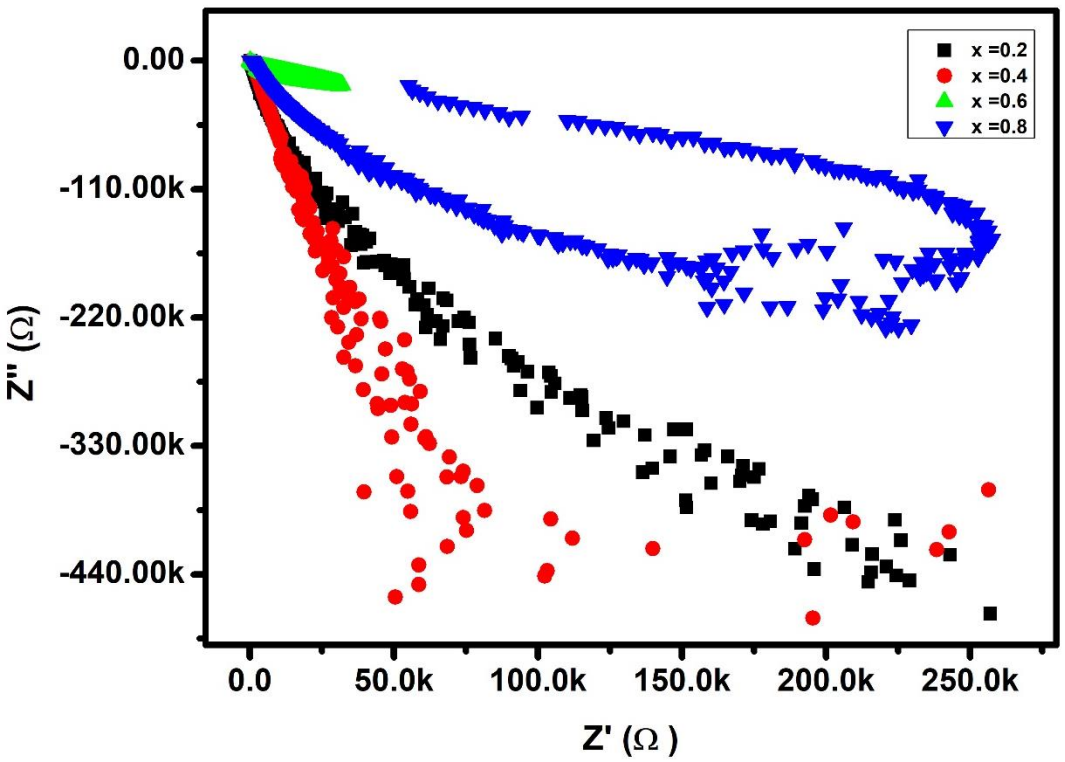

Fig.9 Z' versus Z'' plots of ALTBZF nanocomposites

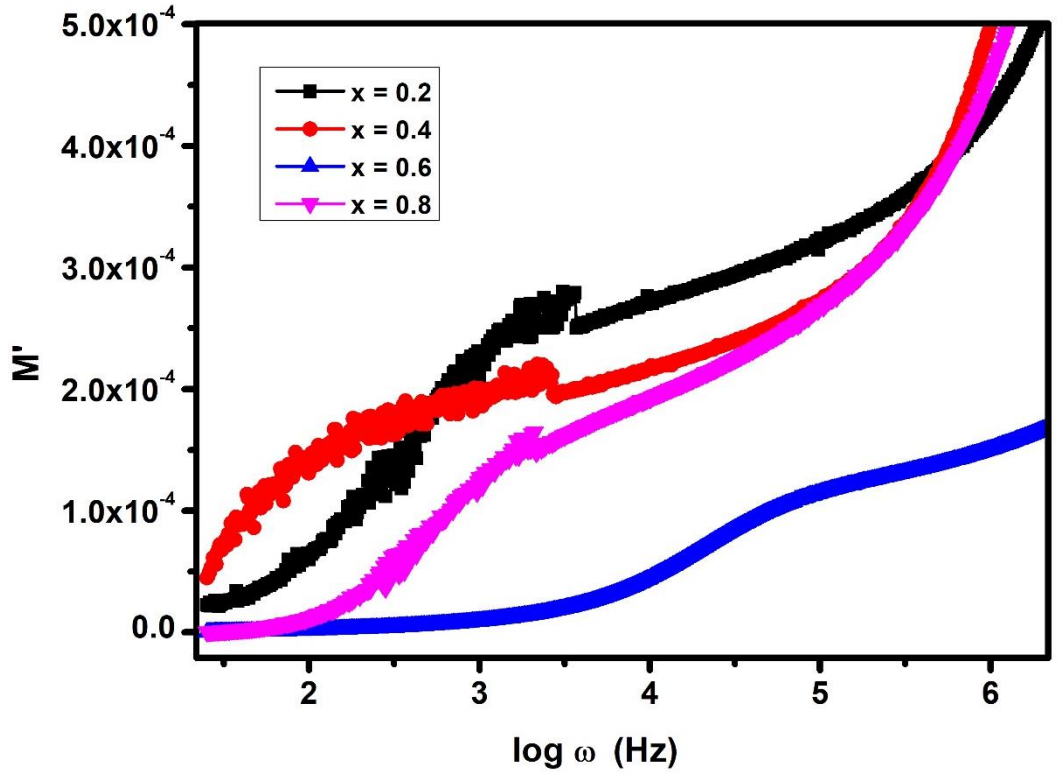

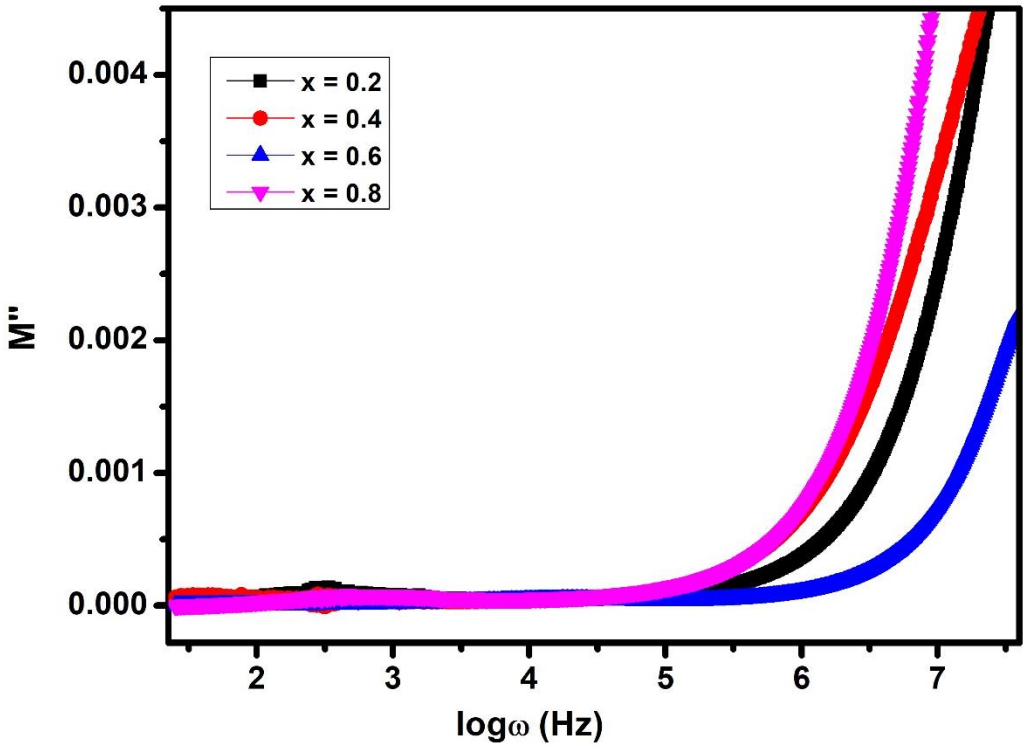

Fig.10 M'- log ω and M''- log ω plots of ALTBZF nanocomposites

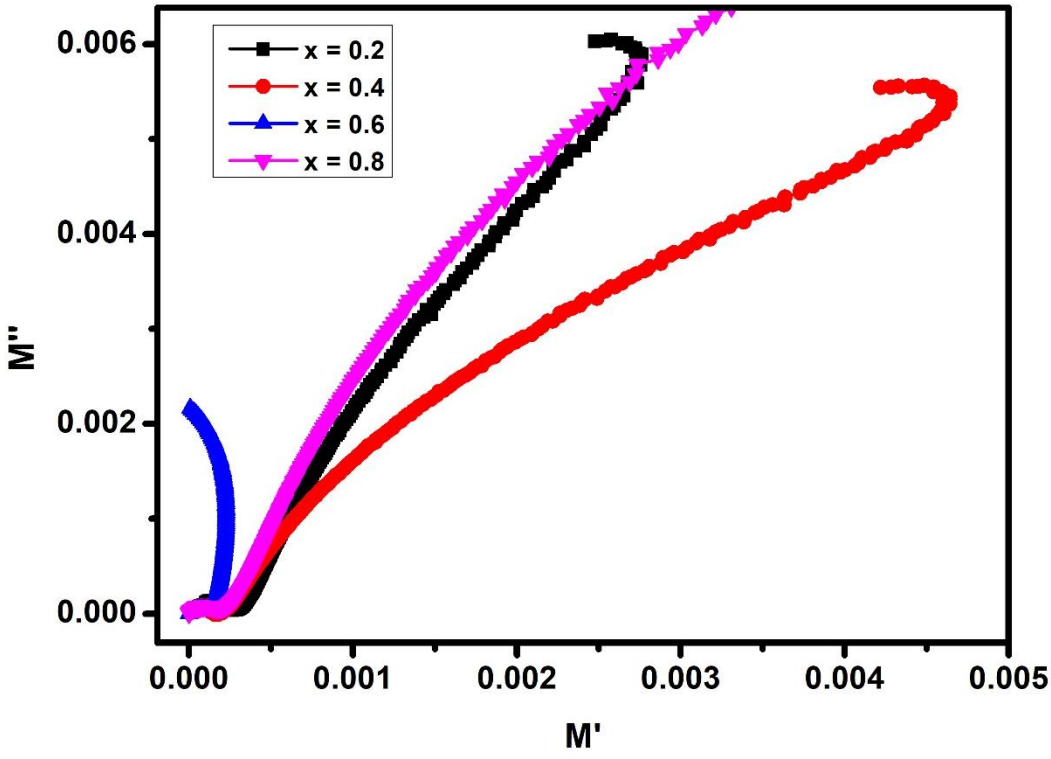

Fig.11 M' versus M'' plots of ALTBZF nanocomposites

4. Conclusions

The ALTBZFO nanocomposites were prepared using the low temperature hydrothermal method. The XRD analysis indicated the structural transformation from tetragonal to cubic for y = 0.2 to 0.4 - 0.8 samples, respectively. The lattice constants for x = 0.2 sample were noted to be a = b = 3.774 Å & c = 9.395 Å. But, for x = 0.4 – 0.8 samples, these lattice constants were decreased from 12.761 to 12.714 Å, respectively. The FESEM, and TEM pictures revealed the generation of nanospheres, and few nanorods in the morphology. The high dielectric constant was obtained for x = 0.2 – 0.8 samples at 1 MHz frequency. Hence, the present nanocomposites were suitable for charge stored capacitor, and perfect absorber applications. Moreover, interestingly, x = 0.6 nanocomposite showed the negative dielectric behavior from 6 to 8 MHz. In addition, the high ac-electrical conductivity was noticed for x = 0.2 – 0.8 samples at 1 MHz. The impedance, and dielectric modulus analysis evidenced the microstructure, and conduction mechanism (behavior of charge carriers).

Conflicts of Interest: The authors declare that we have no conflicts of interest.

Data availability statement: The data will be made immediately available based on the request.

Acknowledgements

The authors express thankfulness to Dr. P. Sreeramulu, Assistant Professor (English), GITAM, Bangalore for providing English language editing services to this manuscript.

References

[1] B. Venkata Shiva Reddy, K. Srinivas, N. Suresh Kumar, K. Chandra Babu Naidu, S. Ramesh, Nanorods like microstructure, photocatalytic activity, and ac-electrical properties of

(1-x) ($Al_{0.2}La_{0.8}TiO_3$) + (x) ($BaTiO_3$) (x = 0.2, 0.4, 0.6 & 0.8) nanocomposites,Chemical Physics Letters 752 (2020) 137552,https://doi.org/10.1016/j.cplett.2020.137552

[2] S. Dastagiri, M. V. Lakshmaiah, K. Chandra Babu Naidu, Defect dipole polarization mechanism in low-dimensional Europium substituted $Al_{0.8}La_{0.2}TiO_3$ nanostructures,Physica E: Low-dimensional Systems and Nanostructures 120 (2020) 114058, https://doi.org/10.1016/j.physe.2020.114058,

[3] B. Venkata Shiva Reddy, K. Srinivas, N. Suresh Kumar, K. Chandra Babu Naidu, Phase transformation, nanorods like morphology, wide band gap and dielectric properties of 1-x ($Al_{0.2}La_{0.8}TiO_3$) + x ($BaTiO_3$) (x = 0.2 - 0.8) nanocomposites,Journal of Materials Science: Materials in Electronics, (2020) https://doi.org/10.1007/s10854-020-03469-6

[4]. S. Dastagiri, M.V. Lakshmaiah, K. Chandra Babu Naidu, N. Suresh Kumar, A. Khan, Induced dielectric behavior in high dense $Al_xLa_{1-x}TiO_3$ (x = 0.2–0.8) Nanospheres. J. Mater. Sci.: Mater. Electron. 30, 20253–20264 (2019)

[5]. A. Mallikarjuna, S. Ramesh, N.S. Kumar, K. Chandra Babu Naidu, K.V. Ratnam, H. Manjunatha, B.P. Rao, Structural transformation and high negative dielectric constant behaviour in (1-x) ($Al_{0.2}La_{0.8}TiO_3$) + (x) ($BiFeO_3$) (x = 0.2–0.8) nanocomposites. Physica E 122, 114204 (2020)

[6]. A. Mallikarjuna, S. Ramesh, N. Suresh Kumar, K. Chandra Babu Naidu, K. Venkata Ratnam, H. Manjunatha, Photocatalytic activity, negative ac- electrical conductivity, dielectric modulus, and impedance properties in 0.6 ($Al_{0.2}La_{0.8}TiO_3$) + 0.4 ($BiFeO_3$) nanocomposite. Cryst. Res. Technol. 55, 1–10 (2020) 202000068

[7]. N. Suresh Kumar, R. Padma Suvarna, K. Chandra Babu Naidu, Negative dielectric behavior in tetragonal $La_{0.8}Co_{0.2-x}Eu_xTiO_3$ (x = 0.01–0.04) nanorods. Mater. Charact. 166, 110425 (2020)

[8]. Klingshirn C, ZnO: material, physics and applications. Chem Phys Chem. **8** (2007) 782–803. doi:10.1002/cphc.200700002

[9]. Bulent Caglar, FatihİÇer, Kemal Volkan Özdokur, Sema Caglar, Agah Oktay Özdemir, Eda Keles Guner, Burcu Meryem Beşer, Ahmet Altay, Çağrı Çırak, Bilge Doğan, Ahmet Tabak, A novel amperometric H_2O_2 biosensor constructed by Cress peroxidase entrapped on $BiFeO_3$ nanoparticles, Materials Chemistry and Physics (2021), 124287 https://doi.org/10.1016/j.matchemphys.2021.124287,

[10]. A.F.Lima, Optical properties, energy band gap and the charge carriers' effective masses of the R3c $BiFeO_3$ magnetoelectric compound, Journal of Physics and Chemistry of Solids 144 (2020) 109484

[11]. Muhamad Kamil Yaakob, Nur Miza Atikah Zulkafli, Muhd Firdaus Kasim, Mohamad Hafiz Mamat, Ahmad Azmin Mohamad, Li Lu, Muhd Zu AzhanYahya, Structural phase instability, mixed-phase, and energy band gap change in $BiFeO_3$ under lattice strain effect from first-principles investigation, Ceramics International (2021), https://doi.org/10.1016/j.ceramint.2021.01.118

[12]. Peilin Yuan, Dabin Li, Lan Wu, Lei Shi, Synthesis and growth mechanism of monodispersed $BiFeO_3$ nanorods with controllable aspect ratio and magnetic/optical properties, Ceramics International 46 (2020) 1243 - 1247

[13]. F.Sánchez-De Jesús, A.M.Bolarín-Miró, C.A.Cortés-Escobedo, A.Barba-Pingarrón, F.Pedro-García, Enhanced ferromagnetic and electric properties of multiferroic $BiFeO_3$ by doping with Ca, Journal of Alloys and Compounds 824 (2020) 153944

[14]. Rida Ahmed, Ren Jun Si, Sajidur Rehman, Yi Yu, Qiu Ju Li, Chunchang Wang, High dielectric constant and low temperature ferroelectric-phase-transition in Ca, Pb co-doped $BiFeO_3$, Results in Physics 20 (2021) 103623

[15]. Wen Dong, Yiping Guo, Bing Guo, Hongyan Liu, Hua Li, Hezhou Liu, Photovoltaic properties of $BiFeO_3$ thin film capacitors by using Al-doped zinc oxide as top electrode, Materials Letters 91 (2013) 359 – 361

[16]. Qing-Yan Rong, Wen-Zhi Xiao, Gang Xiao, Ai-Ming Hu, Ling-Ling Wang, Magnetic properties in $BiFeO_3$ doped with Cu and Zn first-principles investigation, Journal of Alloys and Compounds, 674 (2016) 463 – 469

[17]. Shiju Yang, Fengqing Zhang, Xiaobin Xie, Huajun Sun, Liping Zhang, Suhua Fan, Enhanced leakage and ferroelectric properties of Zn-doped $BiFeO_3$ thin films grown by sol-gel method, Journal of Alloys and Compounds, 734 (2018) 243 – 249

[18]. Jian Liu, Hongmei Deng, Xuezhen Zhai, Tie Lin, Xiangjian Meng, Yuanyuan Zhang, Wenliang Zhou, Pingxiong Yang, Junhao Chu, Influence of Zn doping on structural, optical and magnetic properties of $BiFeO_3$ films fabricated by the sol–gel technique, Materials Letters 133 (2014) 49 - 52

[19]. C.M.Raghavan, J.W.Kim, S.S.Kim, Effects of (Dy, Zn) co-doping on structural and electrical properties of $BiFeO_3$ thin films, Ceramics International 40 (2014) 2281 – 2286

[20]. R.Rajalakshmi, Nagaiah Kambhala, S.Angappane, Enhanced magnetic properties of chemical solution deposited $BiFeO_3$ thin film with ZnO buffer layer, Materials Science and Engineering B, 177 (2012) 908 - 912

[21]. Poonam Uniyal, K.L.Yadav, Synthesis and study of multiferroic properties of $ZnFe_2O_4$–$BiFeO_3$ nanocomposites, Journal of Alloys and Compounds 492 (2010) 406 – 410

[22]. R.D. Shannon, Revised Effective Ionic Radii and Systematic Studies of Interatomic Distances in Halides and Chalcogenides, *Acta Cryst.* **A 32** (1976) 751-767.

[23]. Scherrer, P. Bestimmung der Grosse und der Inneren Struktur von Kolloidteilchen Mittels Rontgenstrahlen, Nachrichten von der Gesellschaft der Wissenschaften, Gottingen. Mathematisch-Physikalische Klasse, 2 (1918) 98-100

[24]. N. Suresh Kumar, R. Padma Suvarna, K.C. B. Naidu, G. Ranjith Kumar, S. Ramesh, Structural and Functional Properties of Sol-Gel Synthesized and Microwave Heated $Pb_{0.8}Co_{0.2-z}La_zTiO_3$ (z=0.05-0.2) Nanoparticles, Ceramics International 44 (2018) 19408-19420

[25]. N. S. Kumar, R. P. Suvarna and K. C. B. Naidu, Sol-Gel Synthesized and Microwave Heated $Pb_{0.8-y}La_yCo_{0.2}TiO_3$ (y= 0.2–0.8) Nanoparticles: Structural, Morphological and Dielectric Properties, Ceramics International 44 (2018) 18189-18199

[26]. K.W. Wagner, The Distribution of Relaxation Times in Typical Dielectrics, Ann. Phys., 40 (1913) 817

[27]. Baba Basha, D. An improved dielectric behavior of hydrothermally synthesized $Ba_{0.4}La_{0.6-y}Eu_yTiO_3$ (y = 0.01–0.04) nanorods. *J Mater Sci: Mater Electron* (2021). https://doi.org/10.1007/s10854-021-05297-8

[28]. Baba Basha, D. Hydrothermal synthesis of $Ba_{1-x}La_xTiO_3$ ($x = 0.2$, 0.4, 0.6, & 0.8) nanorods: structure, morphology, optical band gap, and dielectricity behavior. *J Mater Sci: Mater Electron* 31, 16448–16458 (2020). https://doi.org/10.1007/s10854-020-04199-5

[29]. R.M. De la Cruz, C. Kanyinda-Malu, J.E. Muñoz Santiuste, Dielectric tensor of a rectangular arrangement of Ag nanoparticles in anisotropic $LiNbO_3$: analysis of the negative epsilon conditions. Physica B 581, 411957 (2020)

[30]. D. Schurig, J.J. Mock, D.R. Smith, Electric-field-coupled resonators for negative permittivity metamaterials. Appl. Phys. Lett. 88, 041109 (2006)

[31]. M.A. Rahman, E. Ahamed, M.R.I. Faruque, M.T. Islam, Preparation of $NiAl_2O_4$-based flexible substrates for metamaterials with negative dielectric properties. Sci. Rep. 8, 14948 (2018)

[32]. O. Sakai, A. Iwai, Y. Omura, S. Iio, T. Naito, Wave propagation in and around negative-dielectric-constant discharge plasma. Phys. Plasmas 25, 031901 (2018)

[33]. B. Li, G. Sui, W.H. Zhong, Single negative metamaterials in unstructured polymer nanocomposites toward selectable and controllable negative permittivity. Adv. Mater. 21, 4176–4180 (2009)

[34]. A. Manohar, V. Vijayakanth, R. Hong, Solvothermal reflux synthesis of $NiFe_2O_4$ nanocrystals dielectric and magnetic hyperthermia properties. J. Mater. Sci. 31(1), 799–806 (2019)

Figures

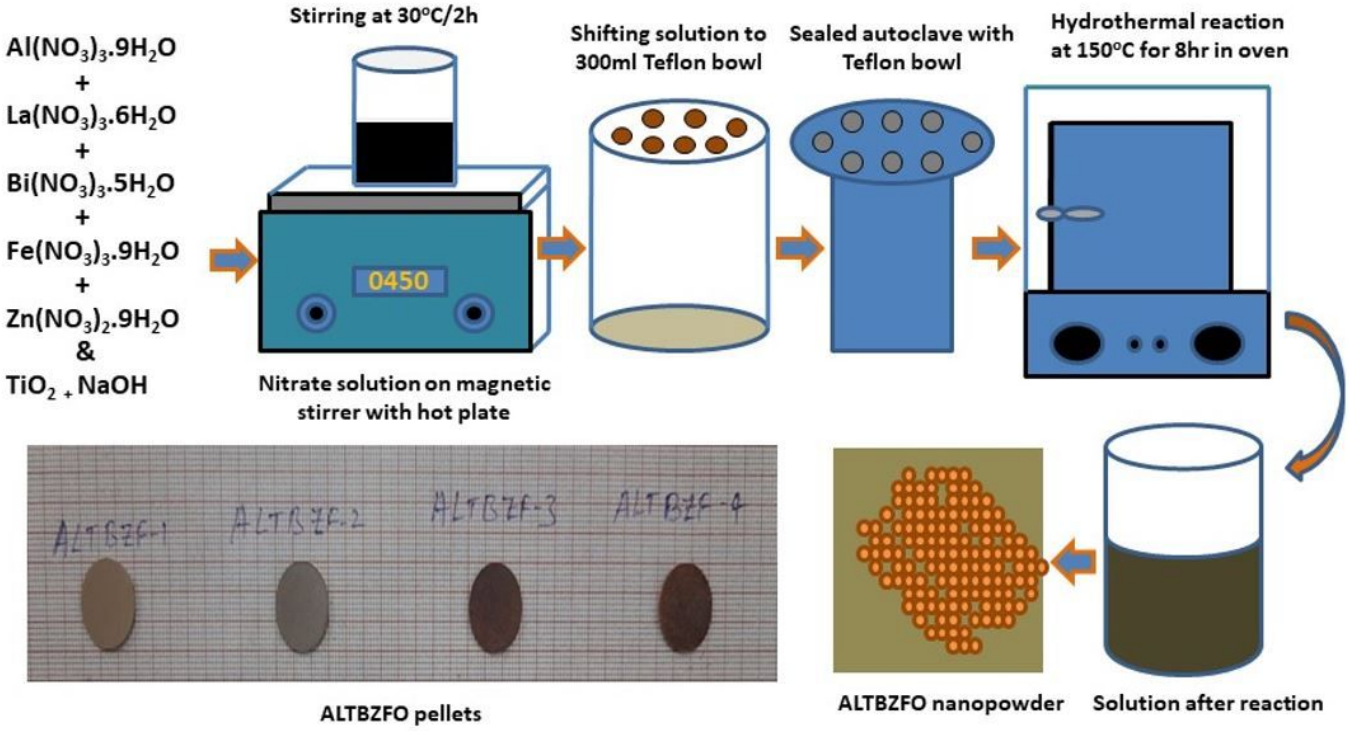

Figure 1

Schematic representation of hydrothermal synthesis and sample preparation

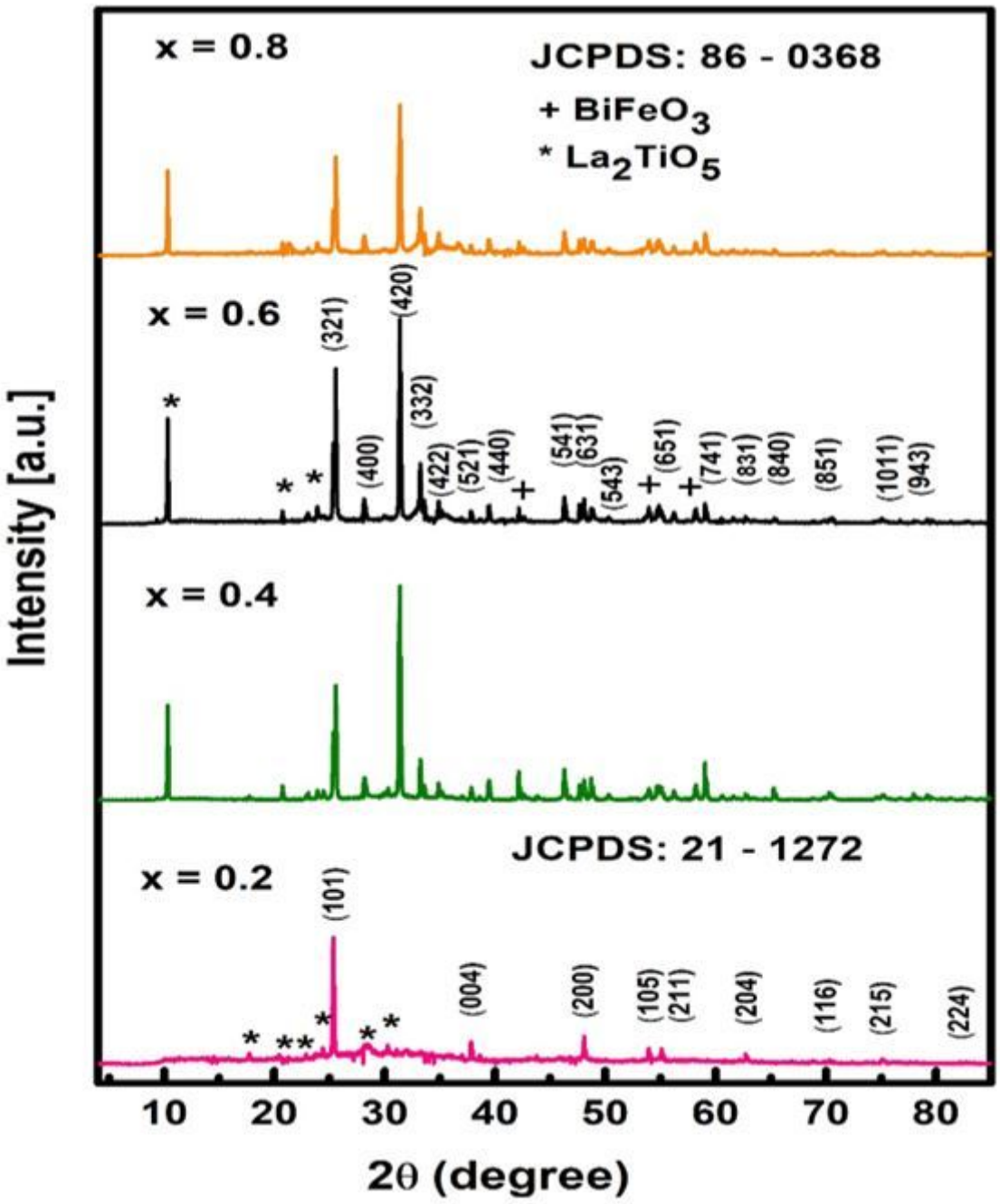

Figure 2

XRD patterns of ALTBZF nanocomposites

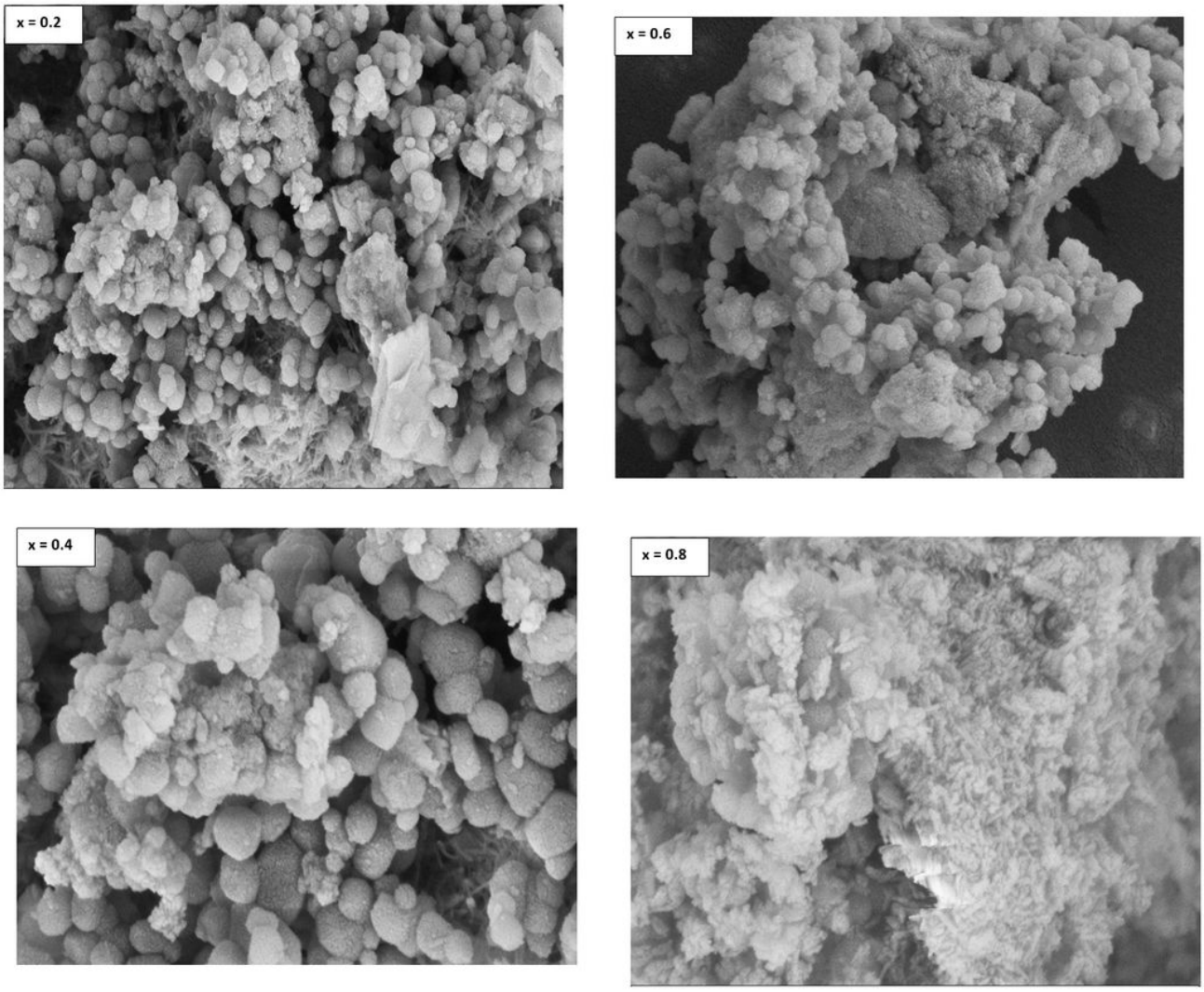

Figure 3

FESEM pictures of ALTBZF nanocomposites

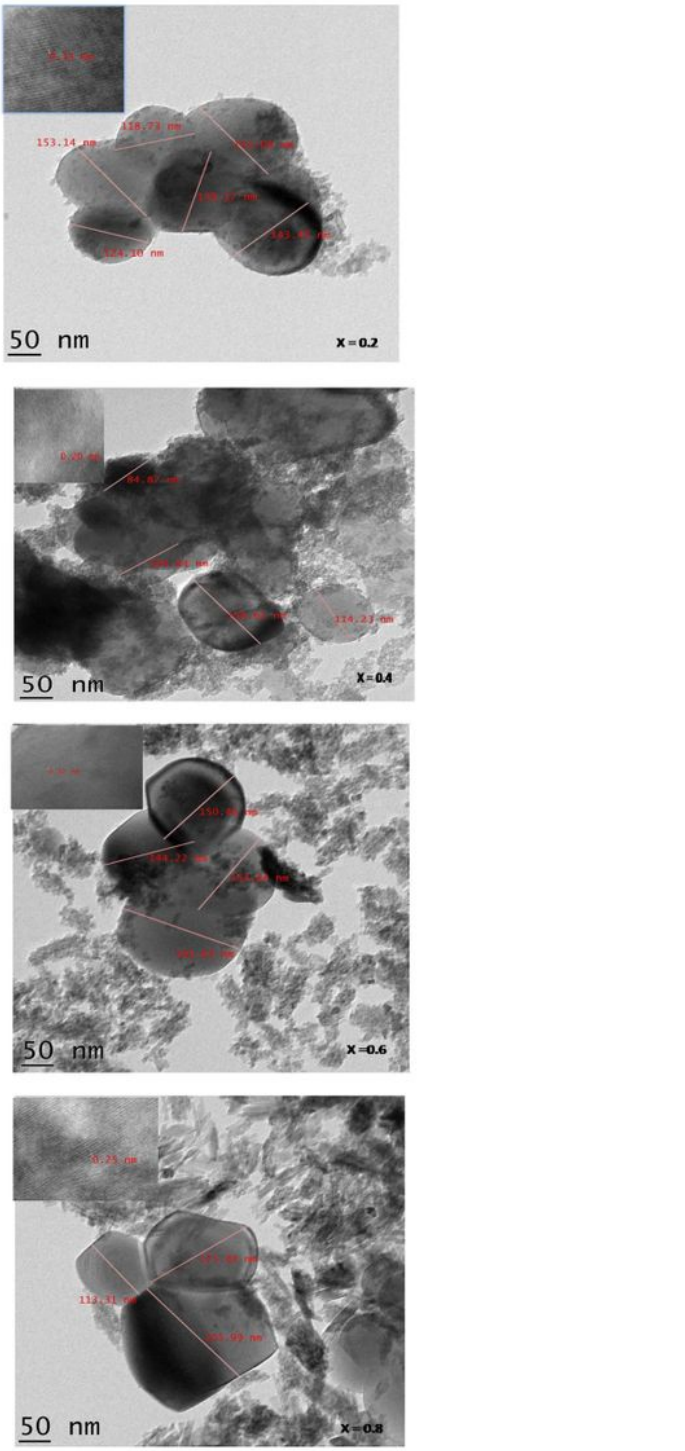

Figure 4

TEM pictures of ALTBZF nanocomposites

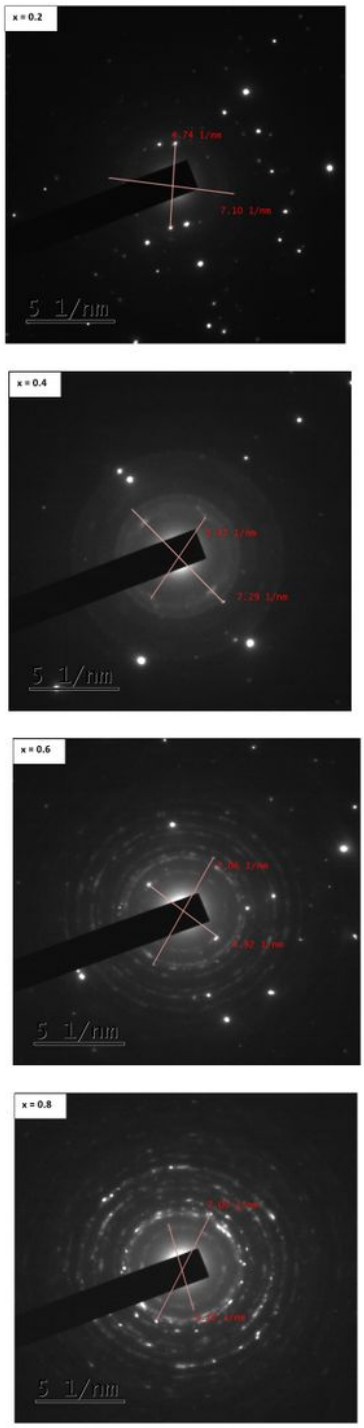

Figure 5

SAED patterns of ALTBZF nanocomposites

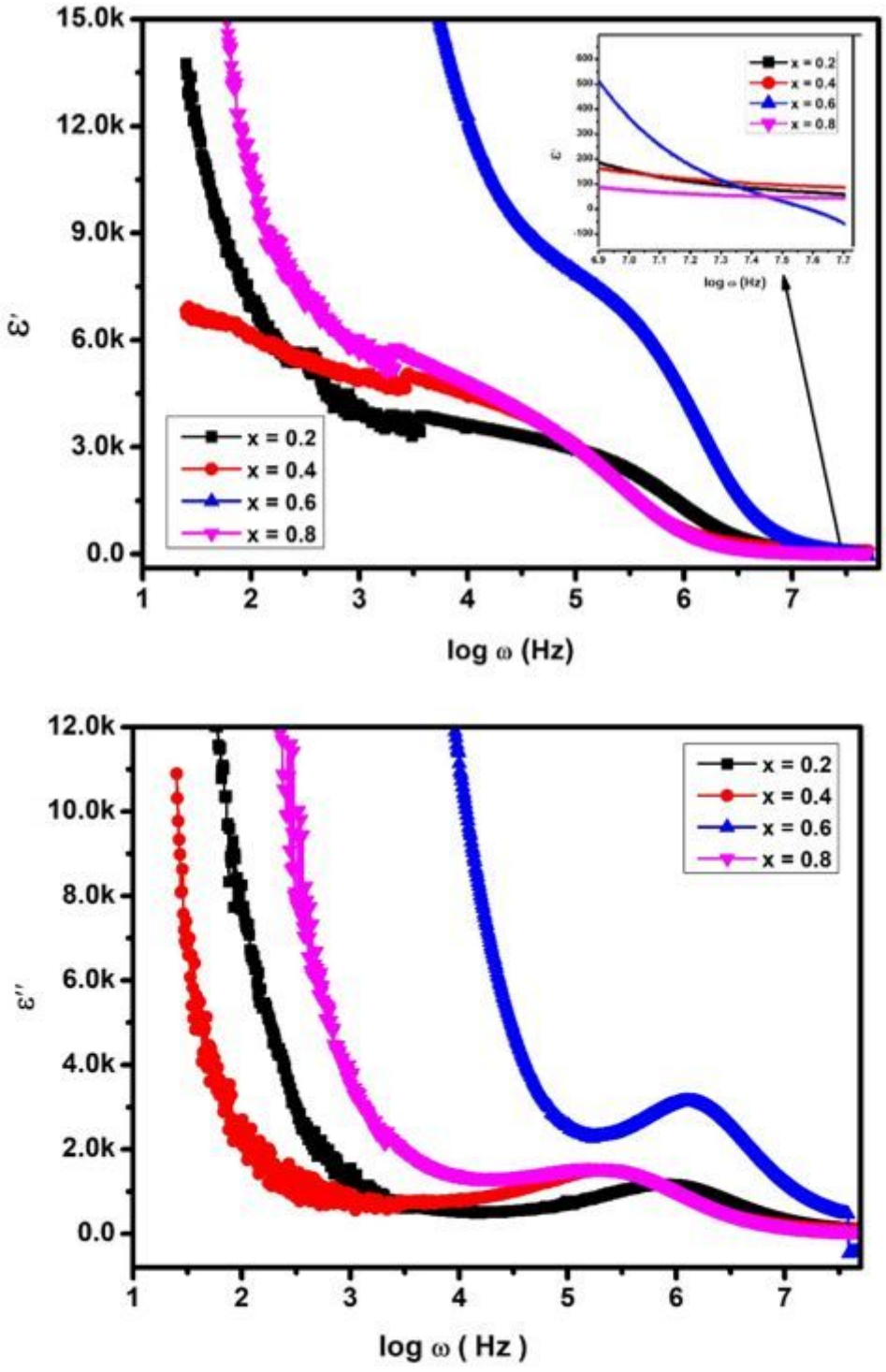

Figure 6

Frequency dependence of dielectric properties of ALTBZF nanocomposites

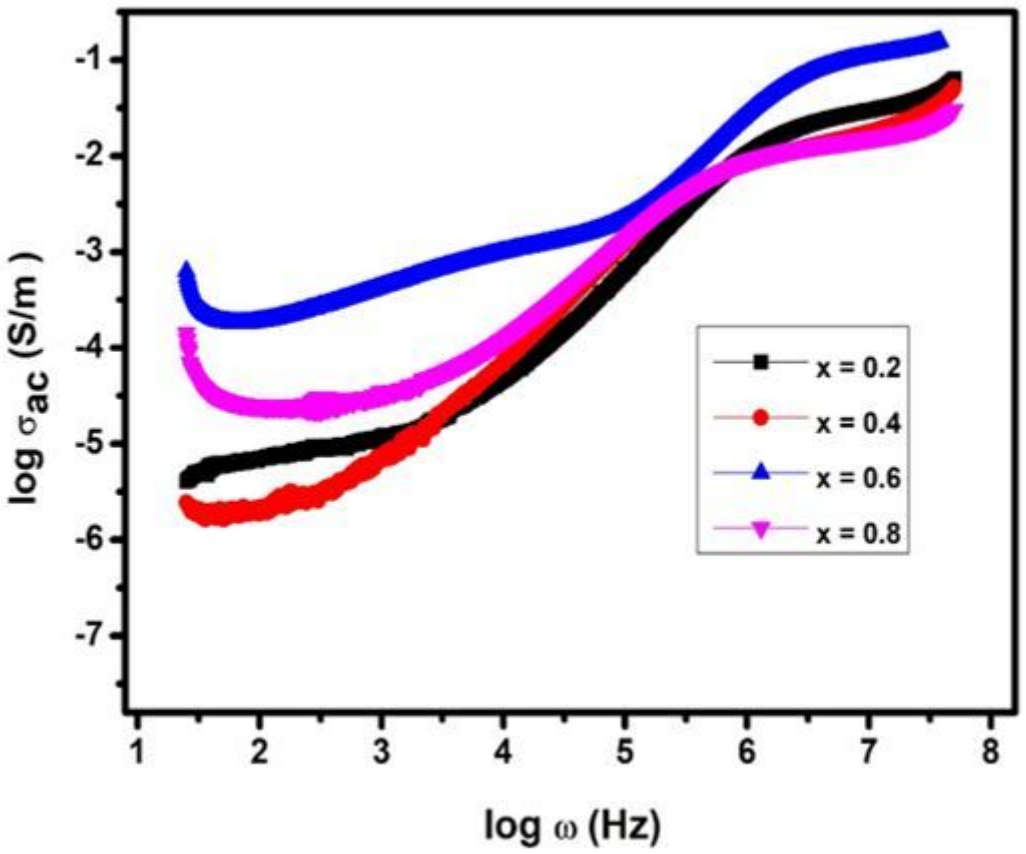

Figure 7

AC- electrical conductivity versus log ω plots of ALTBZF nanocomposites

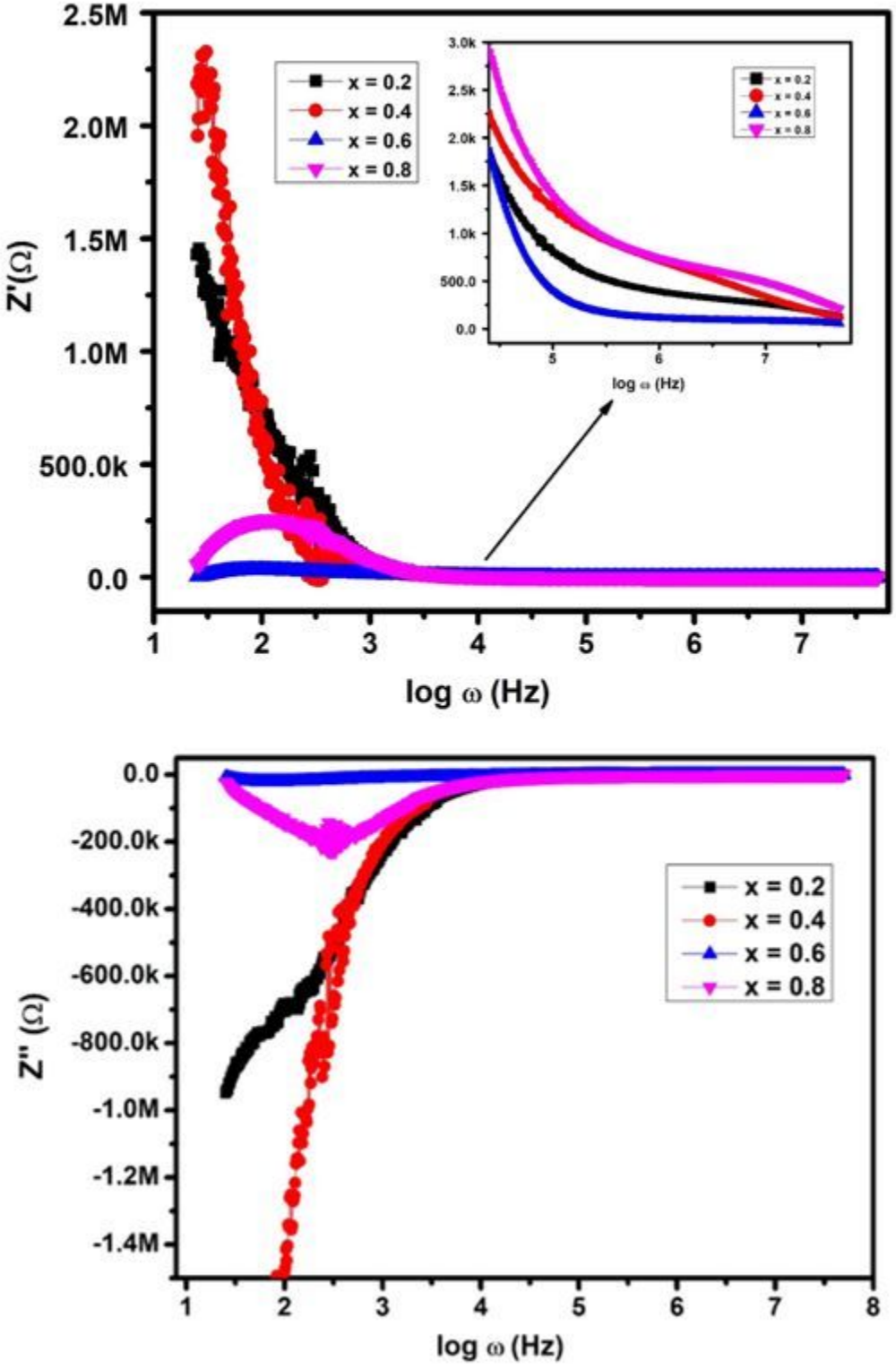

Figure 8

Z'- log ω and Z''- log ω plots of ALTBZF nanocomposites

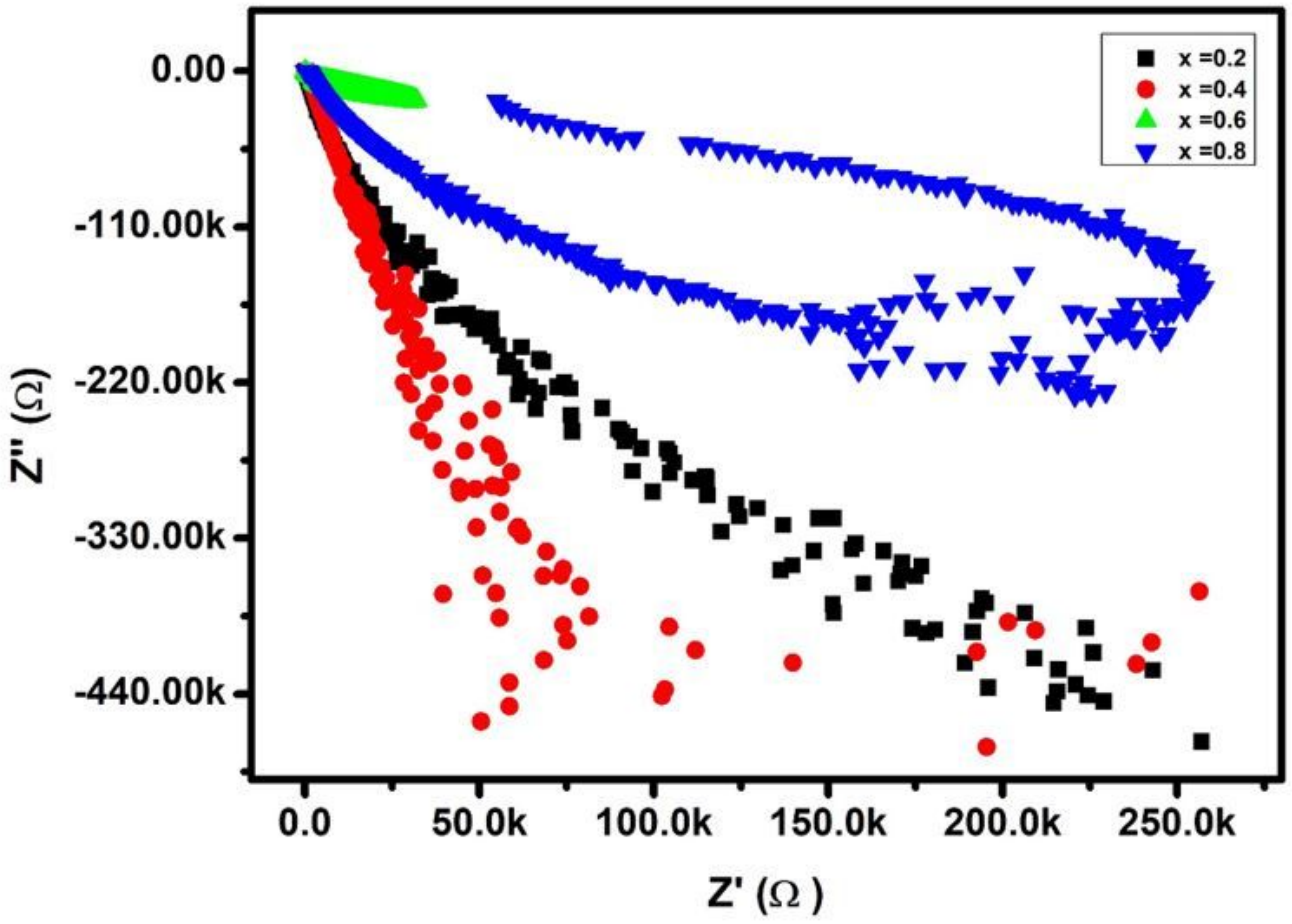

Figure 9

Z' versus Z" plots of ALTBZF nanocomposites

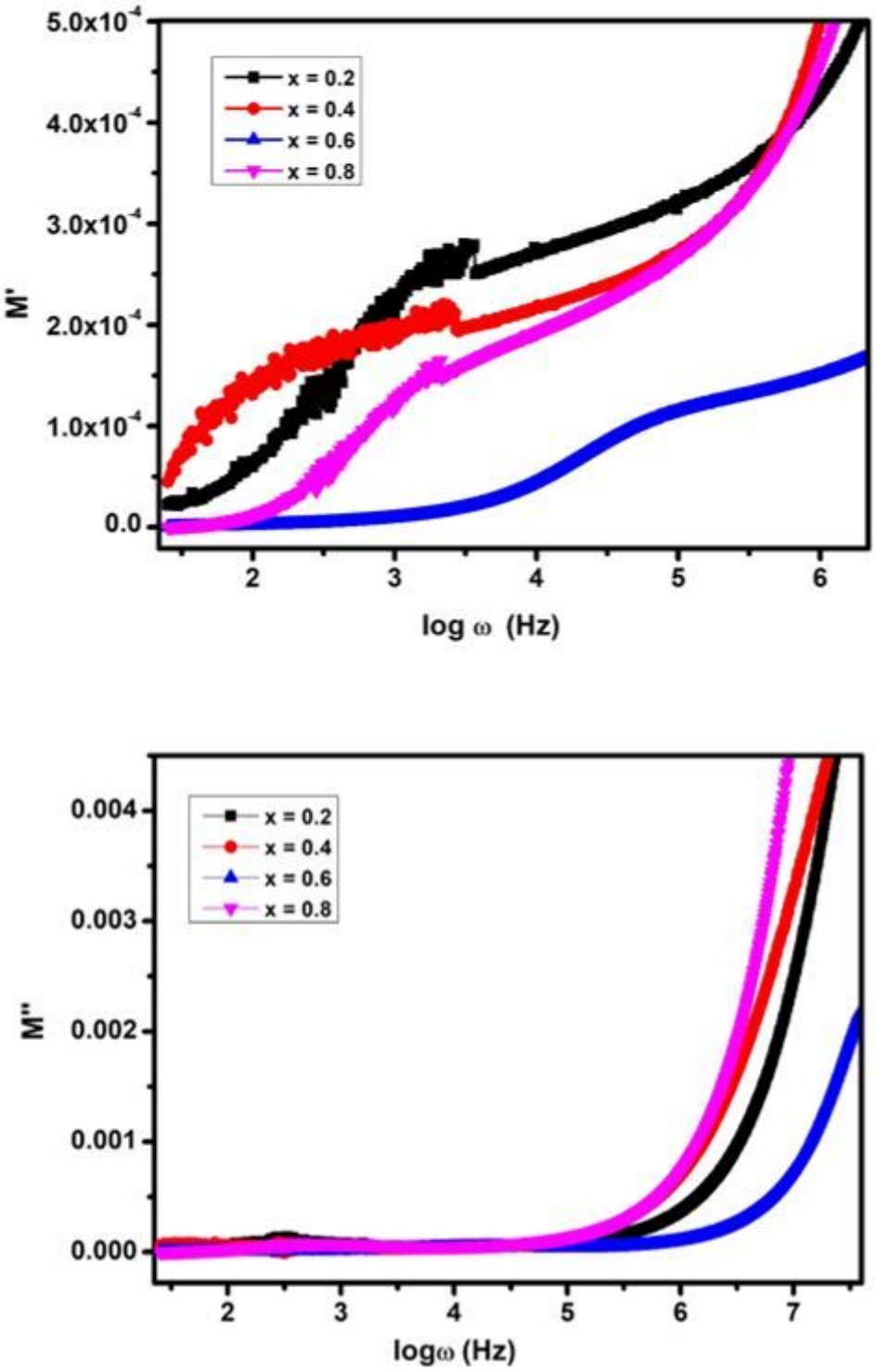

Figure 10

M'- log ω and M''- log ω plots of ALTBZF nanocomposites

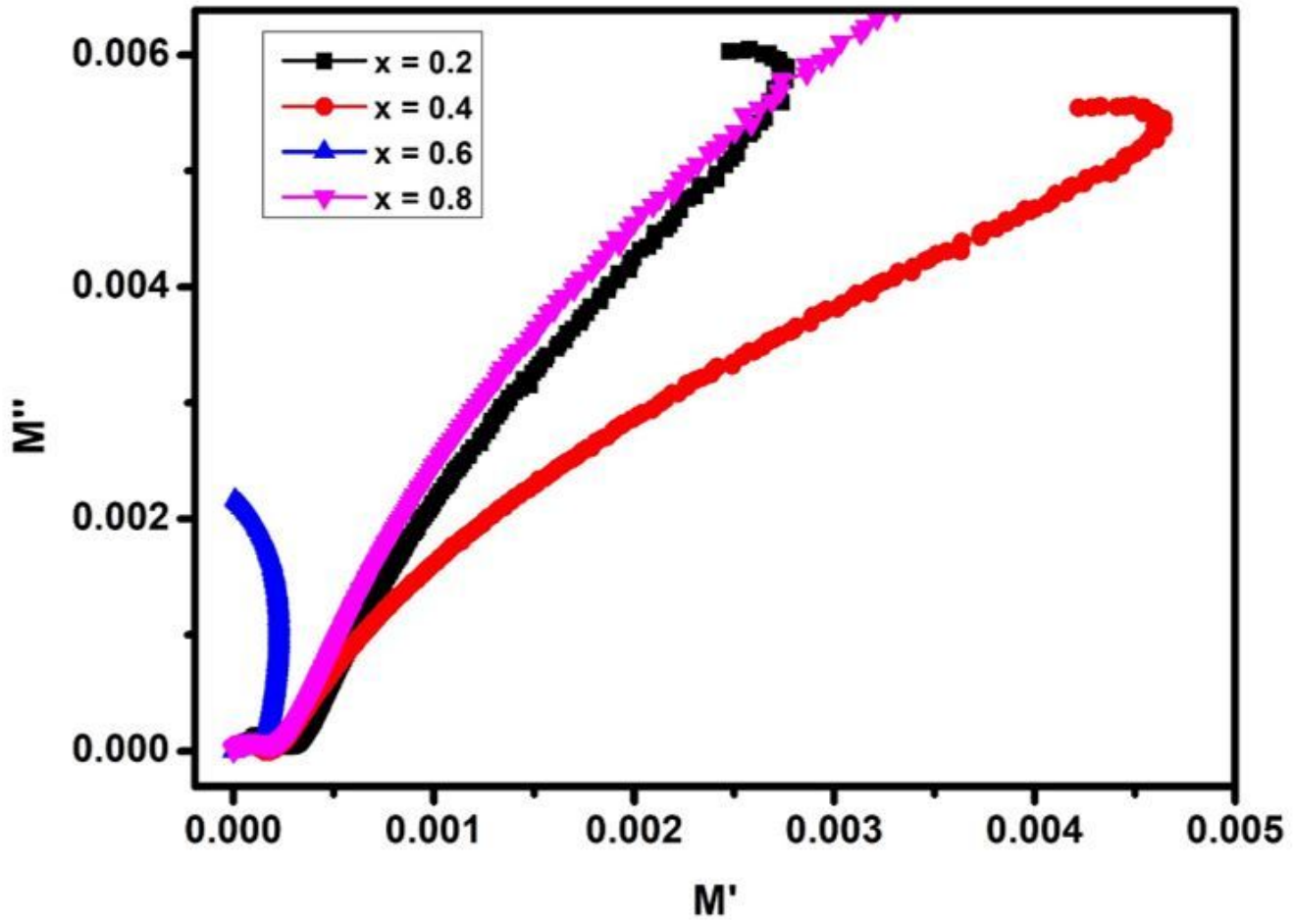

Figure 11

M' versus M'' plots of ALTBZF nanocomposites